https://doi.org/10.5194/egusphere-2026-346
Preprint. Discussion started: 4 February 2026

Tide of the Time: Global tidal characteristics observed from in-situ measurements

Michael G. Hart-Davis[1,*], Roman Sulzbach[2], Stefan A. Talke[3], Ivan D. Haigh[4,5], Marta Marcos[6], Philip Woodworth[7], Richard Ray[8], Ole B. Andersen[9], Florent Lyard[10], Ergane Fouchet[11], Denise Dettmering[1], Maik Thomas[2,12], and Florian Seitz[1]

[1]Deutsches Geodätisches Forschungsinstitut, Technische Universität München, Germany
[2]GFZ Helmholtz Centre for Geosciences, Telegrafenberg, Potsdam, Germany
[3]Department of Civil and Environmental Engineering, California Polytechnic State University, San Luis Obispo, California, USA
[4]School of Ocean and Earth Science, University of Southampton, National Oceanography Centre, Southampton, UK
[5]National Centre for Integrated Coastal Research and Department of Civil, Environmental and Construction Engineering, University of Central Florida, USA
[6]IMEDEA (UIB-CSIC), Esporles, Balearic Islands, Spain
[7]National Oceanography Centre, Liverpool, UK
[8]NASA Goddard Space Flight Center, Greenbelt, MD, USA
[9]DTU Space, Technical University of Denmark, Kongens Lyngby, Denmark
[10]LEGOS, Université de Toulouse, CNES, CNRS, IRD, Toulouse, France
[11]Mercator Ocean International, Toulouse, France
[12]Institute for Meteorology, Freie Universität Berlin, Berlin, Germany
[*]corresponding author: michael.hart-davis@tum.de

Correspondence: Michael G. Hart-Davis (michael.hart-davis@tum.de)

Abstract. Tide gauges have been critical sources for sea level research, enabling the development of tidal theory and an understanding of local variations that occur across the global oceans. Tides play important roles in a variety of oceanographic and geodetic applications, and characterising their spatial variability is valuable for applications ranging from fishing to flood risk management. This manuscript presents the coastal characteristics of ocean tides based on 3,591 high-frequency tide gauge observations from the recently updated GESLA-4 database. These characteristics range from tidal datums such as Mean High Water (MHW) and the Great Diurnal Range to metrics like the Age of the Tide, Form Factors, Dodginess, updated amplitude trend estimates, and new insights into the regional duration of high tides. Our analysis finds that 125 out of 237 long-time series show statistically significant trends in one or more constituents, from -1.47 mm/yr to +1.80 mm/yr, while the duration of the high-water stand during spring tides is shown to vary from 1 to 14 hours, for an inundation depth of 20 cm. It is anticipated that the results presented will be useful not only to tidal experts but also to a wide range of cross-disciplinary researchers and local communities, aiding their understanding of a vital component of the global Earth system.

https://doi.org/10.5194/egusphere-2026-346
Preprint. Discussion started: 4 February 2026

1 Introduction

Tides are a persistent and dominant force shaping the coastal zone, shelf seas, and open ocean. They modulate storm surges and waves (Horsburgh and Wilson, 2007), influencing extreme sea levels, flooding, and erosion (Pugh and Woodworth, 2014), constrain navigation and port access (Akan et al., 2017), and govern vertical ecological zonation in intertidal environments (Stumpf and Haines, 1998). In the open ocean, tidal dissipation affects large-scale circulation and vertical mixing (Munk, 1966; Wunsch and Ferrari, 2004; Green et al., 2009). Across shelf seas, tides drive sediment dynamics (Simpson and Sharples, 2012) and underpin tidal energy resources (Robins et al., 2015) and generate coherent turbulence (Smith et al., 1999; Talke et al., 2013), enhancing mixing and air–sea gas exchange (Talke et al., 2013; Zappa et al., 2007), with consequences for carbon dioxide uptake (Thomas et al., 2004) and hypoxia (Talke et al., 2009). Recent studies have shown that multi-year to decadal tidal cycles modulate the frequency of both extreme flood return levels and high-tide flooding (Enríquez et al., 2022; Thompson et al., 2021). In estuaries, interactions among tides, mixing, and river discharge regulate salinity intrusion (Jay, 1991; Geyer and MacCready, 2014), sediment transport, and system morphology, shaping mass, momentum, and energy budgets across the river–estuary–shelf continuum (Jay, 1991; Burchard et al., 2018). Tides also shape river plumes (Horner-Devine et al., 2009) and shelf sea fronts, influencing productivity and fisheries (Simpson and Hunter, 1974). Tidal datums underpin many national boundaries and historical geodetic systems (Shalowitz, 1964). Consequently, tides have significant scientific and practical implications.

Tides have been measured since the 17th century, and tide predictions based on the phases of the Moon and empirical knowledge were made much earlier. Cartwright (1999) discusses early understanding of the nature of ocean tides dating back to ancient civilizations, roughly 2000 BC, while Woodworth (2023) discusses the transformation in tidal science thanks to Newton. Systematic tide-gauge measurements have been collected for more than three centuries, providing one of the longest instrumental records in geosciences. Early tide gauges, installed in major European ports in the 17th and 18th centuries, used simple float or staff mechanisms to record water levels relative to fixed benchmarks. By the late 19th century, standardized stilling-well gauges enabled continuous, high-precision tidal observations, forming the foundation of national networks. The transition to automated digital systems in the late 20th century, which are based on pressure, acoustic, or radar technologies, expanded spatial coverage and improved temporal resolution, supporting modern sea-level research, operational forecasting, and coastal hazard assessment. Concepts such as "the high-water mark" and "ordinary high water" held legal significance but were often nebulous in definition, sometimes leading to disputes over property rights. More scientific measurement and analysis approaches were developed by Whewell (1830s) and William Thomson (1872), in particular, the method of harmonic analysis (more on this later). The increasing scientific rigour led to the introduction of concepts such as mean sea level, mean tidal range, and mean high water, which are rigorously defined and provide first-order statistics on how the ocean interacts with land, and how this varies regionally and globally.

The past 75 years has produced many variations on, and alternatives to, conventional harmonic analysis and tidal prediction, including the response method (Munk and Cartwright, 1966), developments on traditional harmonic analysis programs (Godin, 1972; Foreman, 1977; Pawlowicz et al., 2002; Leffler and Jay, 2009; Codiga, 2011), non-stationary analysis approaches (Jay

https://doi.org/10.5194/egusphere-2026-346
Preprint. Discussion started: 4 February 2026

and Flinchem, 1997; Matte et al., 2013; Pan et al., 2018; Lobo et al., 2024; Monahan et al., 2025), inclusion of derivative constraints (Doodson, 1951; Foreman and Henry, 1979), and other statistical and data processing innovations (e.g., Gan et al., 2021; Su and Jiang, 2023). Moreover, the advent of the digital age and the increasing commitment of many countries to open data have led to the increasing size and data coverage of international tide databases, including that of the World Ocean Circulation Experiment (WOCE) project in the 1990s, the University of Hawaii Sea Level Centre (UHSLC), and, more recently, the community-led Global Extreme Sea Level Analysis (GESLA) database (Woodworth et al., 2017; Haigh et al., 2022). Currently, the GESLA-4 database contains around 130,000 station years of data, spanning 6,474 sites (the total unique data is approximately 20-30% less, as many gauge data sets are duplicated). Despite these efforts, available data does not cover all parts of the global coastlines due to either a lack of public data sources or a lack of tide gauges.

With the recent update to GESLA-4, an opportunity arises to evaluate global-scale coastal tidal characteristics using increased coverage spanning 119 countries and extended time series. In this work, we present a variety of popular tidal characteristics, such as tidal range, tidal band, mean high water, and form factor, as well as new statistics, including high tide duration, Dodginess, and updated tidal trend estimates. These insights are valuable for a wide range of users, from coastal communities to ocean modellers.

2 Data and methodology

The GESLA project was established to expand global access to hourly and higher-frequency sea-level records, assembling diverse datasets from a range of sources into a common, quality-controlled format to support research on extreme sea levels. The first release, GESLA-1 in 2009, included 21,197 years of data from 675 records and was used in studies of global sea-level extremes (e.g., Menéndez and Woodworth, 2010; Hunter et al., 2017; Marcos et al., 2015) and in the IPCC Fifth Assessment Report. To improve coverage and incorporate new observations, GESLA-2 was compiled in 2015–2016 (Woodworth et al., 2017), expanding the dataset to 39,151 years from 1,355 records. GESLA-2 supported extensive research on extreme sea levels, tidal and nontidal interactions, flooding hazards, tidal variability, and model validation, and has contributed to the IPCC Special Report on the Ocean and the Cryosphere and the Sixth Assessment Report.

The third version, GESLA-3, released in 2021 (Haigh et al., 2022), represented a major upgrade: it nearly quadrupled the number of records and doubled the total observation years. GESLA-3 comprised 91,021 years of data from 5,119 tide-gauge sites drawn from over 30 global data providers. GESLA-3 refined data processing, added additional metadata, applied uniform format standards, and adhered to FAIR data practices, making it more robust for future research. The most recent and fourth version, GESLA-4, released in 2025 (Haigh et al., 2026), is a compilation of hourly and higher-frequency measurements from 45 agencies across 119 countries, totaling 127,623 station years of data from 6,474 sites. The oldest records date back to the 19th and early 20th centuries, with the oldest gauge dating back to 1 January 1800 in Gorinchem, the Netherlands. However, the majority of records date back to the last 20-50 years.

Tide gauges have been a remarkable source of data for studying ocean tides. The standard technique for determining the astronomical tidal component of a tide gauge record is known as the harmonic method. This technique originated in the work

https://doi.org/10.5194/egusphere-2026-346
Preprint. Discussion started: 4 February 2026

of William Thomson (Lord Kelvin) and George Darwin in the 19th century, building on the insights of Pierre-Simon, Marquis de Laplace. It replaced the earlier non-harmonic methods, which were particularly computationally intensive for their time. Subsequent developments have made the harmonic method the most common technique used by present-day tidal researchers, although alternative approaches, such as various forms of the response method, have been used in some applications. A history of how these methods originated can be found in Cartwright (1999).

The harmonic method parametrises the tide as the sum of N harmonic terms as follows:

$$\text{Tide} = Z_0 + \sum_{i=1}^{N} f_i H_i \cos\left(\omega_i t + V_i + u_i - G_i\right), \tag{1}$$

which is a function of time t. The H_i and G_i are the amplitude and phase lag, respectively, for a particular constituent i with angular frequency ω_i. The term V_i is the equilibrium argument at the origin of time, which thereby provides a connection to the relevant astronomical motions (e.g., Doodson, 1921). The "nodal corrections" f_i, u_i adjust a constituent's amplitude and phase for modulations induced by the 18.6-year motion of the Moon's node (and for some terms the 8.8-year motion of the Moon's argument of perigee); in principle these modulations could be handled directly by a more complete harmonic expansion involving a larger N (e.g., Foreman and Neufeld, 1991), but in practice this is rarely done and the f_i, u_i adjustments are standard. Z_0 refers to the mean sea level. For more details, see Doodson and Warburg (1941); Parker (2007); Pugh and Woodworth (2014); Egbert and Ray (2017). Permitted values of angular frequency are combinations of six fundamental frequencies associated with the orbits of the Moon and Sun (Doodson, 1921). In practice, only the terms with the largest amplitudes in the 'tidal potential' (the gravitational forcing that drives the tides) tend to result in the largest amplitudes in the real ocean. A few dozen terms are usually sufficient for parameterizing the tide in a one-year record to good accuracy; the default standard for NOAA tide prediction is $N = 37$ (Parker, 2007). In nonlinear regimes, many more terms may be required (for example, NOAA uses 120 constituents at Anchorage, Alaska). Most analysts tend to use a set of N terms that work best for their region.

For historical reasons, each major term has a 'name' which originated in the 19th-century work of Kelvin and Darwin. The largest term at most locations is M_2, being the principal semidiurnal component due to the Moon. Its period is half a lunar day. Similarly, S_2 is the principal semidiurnal component due to the Sun, with a period of half a solar day. The tide also has diurnal components; the largest at most locations are K_1 and O_1. The former stems from a combination of both lunar and solar forcings, while the latter is purely lunar. Terms with names such as M_4 and M_6 result primarily from frictional effects at coastal margins and shallow estuaries, and have periods of $1/4$ and $1/6$ of a lunar day (the subscript denotes the approximate number of times a constituent repeats per day). Table 1 presents eight of the major components and their associated periods, while Parker (2007) provides a more comprehensive list.

The dominant tidal constituents commonly found in most parts of the ocean are readily identified by power spectral density analysis, as in Figure 1, which shows high power at similar frequencies in two gauges even though they are in different ocean regions. Particularly evident are peaks in the diurnal (daily) and semi-diurnal (twice daily) bands, corresponding to the primary astronomical forcings. The amplitudes and phase lags of each of these terms at a particular location are calculated by fits to a tide gauge record, generally using least-squares techniques. Once calculated, the set of H and G values (referred to as 'harmonic constants') can be used to calculate the tide far into the future (or past). In fact, the 'constants' at most places tend

https://doi.org/10.5194/egusphere-2026-346
Preprint. Discussion started: 4 February 2026

Table 1. Major tidal constituents and their characteristics

Constituent	Doodson Number	Period (hours)	Brief Description
M_2	255 555	12.421	Principal Lunar Semi-Diurnal Tide
S_2	273 555	12.000	Principal Solar Semi-Diurnal Tide
N_2	245 655	12.658	Larger Elliptical Lunar Semi-Diurnal Tide
K_2	275 555	11.967	Lunisolar Semi-Diurnal Tide
O_1	145 555	25.819	Principal Lunar Diurnal Tide
Q_1	135 655	26.868	Larger Elliptical Diurnal Tide
P_1	163 555	24.066	Principal Solar Diurnal Tide
K_1	165 555	23.934	Principal Lunisolar Diurnal Tide

not to be absolutely constant. Instead, they exhibit seasonal and interannual variability, primarily driven by meteorological factors, and can even change over decades or more, as discussed in Section 6. Variability can also be caused by inaccuracies in measured water levels or time (e.g., Zaron and Jay, 2014). Nevertheless, one can usually analyse a tide gauge record to arrive at a 'best set' of such constants.

In this context, the harmonic analysis approach was employed to create a database of fifty tidal constituents, known as TICON-4 (Hart-Davis et al., 2025), based on the GESLA-4 database, which is utilized to generate the results presented throughout the present paper. To achieve the highest accuracy in outputting tidal constituents, restrictions were placed on the number of observations required for each tide gauge: tide gauges must have had at least 1 year of measurements. In gauges with longer time series but less than 3 years, restrictions were placed on the percentage of available data, valid observations within that time series. For more information on this, see Hart-Davis et al. (2025). Once this was completed, TICON-4 was left with 4,838 tide gauges spread globally, which was further reduced to 3,591 in our study by removing data from rivers and lakes, as well as from regions such as the Baltic Sea and the Red Sea, which are characterized by negligible tides.

The reconstruction of the tidal sea surface heights can be performed by evaluating Equation 1 at arbitrary past or future epochs. Prediction methods generally employ more harmonics than can be estimated from measurements, especially if the original time series is short. Standard methods of "tidal inference" have been developed for this (Parker, 2007). Equivalent to employing these methods, including standard nodal corrections f_i, u_i, subsequent predicted tidal elevations can also be computed with a matrix formalism laid out in Appendix A. This technique has been previously employed to compute tides in space geodesy (Kvas et al., 2019), and it encodes the long periodic variations of tidal phases and amplitudes of the so-called pivot tides (here: $N = 50$), by implicitly estimating a larger number M of minor partial waves from the tide-generating potential. As with inference methods, the elements of the matrix are derived by assuming that the ocean tide admittance varies only weakly with tidal frequency and is quasi-constant for tidal constituents (linear admittance). Here, we consider all minor waves to a threshold of $0.001\,\mathrm{m^2\,s^{-2}}$ from the HW95 tide-generating potential, which amounts to 148 spectral lines (Hartmann and Wenzel, 1994, 1995, see Appendix A).

https://doi.org/10.5194/egusphere-2026-346
Preprint. Discussion started: 4 February 2026

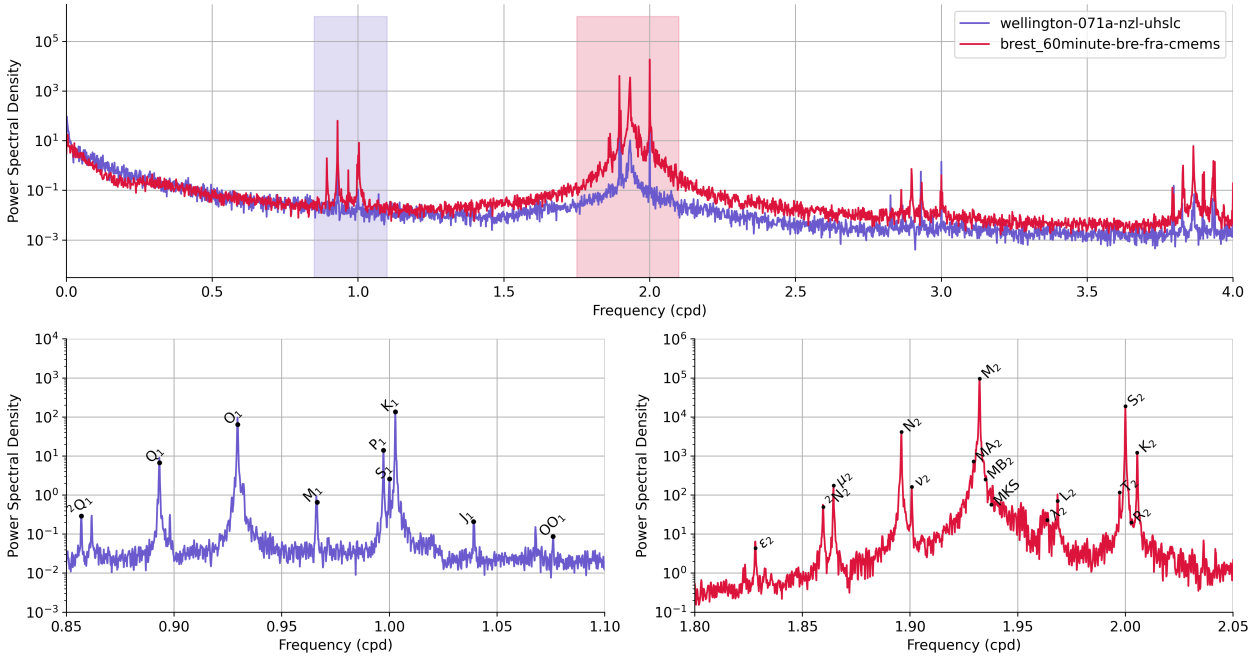

Figure 1. Spectral analysis of the Wellington and the Brest tide gauge, as well as zoom-ins to the semi-diurnal and diurnal band of the Brest gauge, highlighting several tidal constituents.

Both tide-gauge measurements and tidal predictions can be used to characterize tidal regimes through various statistical properties and a number of standard "tidal datums," such as mean low water (MLW). Although most tidal datums are traditionally based on water-level measurements, usually over a complete nodal cycle, we here use tidal predictions based on the TICON-4 constants (as outlined in Appendix A). This allows us to include many tide gauges with a duration of less than 19 years, but always at least one year (a TICON-4 restriction to ensure the highest-accuracy constituents). It also removes from the computed datums any possible non-tidal oceanographic effects, although in most cases these are not expected to be noticeable. Our tidal predictions extend over 200 years, from 1900 to 2100, sampled every 15 minutes. For each time series, we identify tidal highs and lows as local extreme values. From the series of extreme values, we compute the overall highest and lowest astronomical tide (HAT and LAT) and the maximum tidal range as the difference between them.

Additionally, the computed values include the mean high water (MHW) and mean higher high water (MHHW), which is the average of the higher high water of each two consecutive maxima (equivalently for low waters: MLW and MLLW). Together, these tide levels provide a comprehensive description of the tidal regime and the intertidal zone, which allows drawing connections to local biological and geological processes, e.g., the habitability for specific species or the boundary conditions of sedimentation processes. For example, knowledge of local tide levels is important for interpreting Sea Level Index Points related to a specific intertidal zone in sea level reconstruction (e.g., Hijma et al., 2015).

https://doi.org/10.5194/egusphere-2026-346
Preprint. Discussion started: 4 February 2026

3 Tidal constituents

It is not uncommon to see tidal investigations focus on only the eight 'major' constituents. The importance of these eight tides (listed in Table 1) is highlighted in Figure 2, where the median variance explained for each constituent globally is presented. The principal semi-diurnal lunar tide, M_2, unsurprisingly explains the largest percentage of variance, 62.0%, and is shown to be the constituent with the largest tidal amplitude for tide gauges throughout the global oceans.

The eight major tidal constituents (Table 1) explain a total of 74.8% and are found to have larger tidal amplitudes compared to the remaining tidal constituents for 88.1% of tide gauges globally. Despite the significant influence of the semi-diurnal components, there are known regions, such as the Gulf of Mexico and the southwest coast of Australia, that are dominated by the diurnal constituents. While our analysis focuses on coastal tide gauges, the derivation of tidal constituents can be influenced by nontidal processes, such as river dynamics (this is expanded upon in Section 7). This can result in some gauges where this analysis is performed showing dominant tidal constituents that are unexpectedly dominated by smaller constituents, such as K_2 and P_1, which could be a result of the influence of nontidal processes.

Despite the importance of major tides, the remaining tidal constituents—the 'minor' tides—are still of considerable importance (Egbert and Ray, 2017). Based on TICON-4, we calculate that the amplitude of at least one minor tide exceeds that of the major tides in 15.0% of coastal tide gauges; when evaluating gauges within rivers only, this increases to 50.5%. In Figure 3C, the largest minor tide from each tide gauge is presented, with the cumulative counts presented in Figure 3A. The ν_2, M_4, and μ_2 constituents are revealed as the most dominant minor tides, which are observable throughout the global coasts. The ν_2 and μ_2 being of such importance is particularly crucial, as studies by Hart-Davis et al. (2021) have discussed the challenges of estimating these constituents from satellite altimetry within global ocean tide models, due to signal-to-noise issues and perturbations from nonlinear effects. In many global models, these two constituents are accounted for in tidal prediction by inferring them via admittance approaches. The MA_2 and MB_2 are particularly important in higher latitudes along the Canadian coast (Figure 3C), as these constituents are manifestations of the seasonal variability of the M_2 tide, which is caused by various factors, including sea ice cover (Ray, 2022).

Shallow water constituents form as a result of nonlinear interactions with major tidal constituents, causing asymmetry in the tidal waves and leading to their formation. The physical mechanisms underlying the appearance of nonlinear constituents are reviewed in detail by Le Provost (1991). The M_4 constituent, a fundamental harmonic of the major M_2, is known to reach large amplitudes in some shelf waters, exceeding 50 cm in the Bristol Channel, and it is identified in Figure 3A as one of the largest minor constituents. Several shallow-water tides, such as the $2SM_2$ and $2MS_6$, exhibit amplitudes exceeding 2 cm at many tide gauges, highlighting not only the complexity of tides in local regions but also the value of tide gauges in resolving these tides. From a data-derived tide modelling standpoint, resolving these shallow water tides is rather challenging, with state-of-the-art models deriving only a handful of the largest of these constituents (Lyard et al., 2021).

Some recent efforts in the modelling community have begun work on the long-neglected third-degree tidal constituents (Woodworth, 2019; Ray, 2020; Sulzbach et al., 2022). These tides result from a small asymmetry in the tidal potential, and in the diurnal and semidiurnal bands they can be detected most readily only in long (> 8-year) time series. Although observed

https://doi.org/10.5194/egusphere-2026-346
Preprint. Discussion started: 4 February 2026

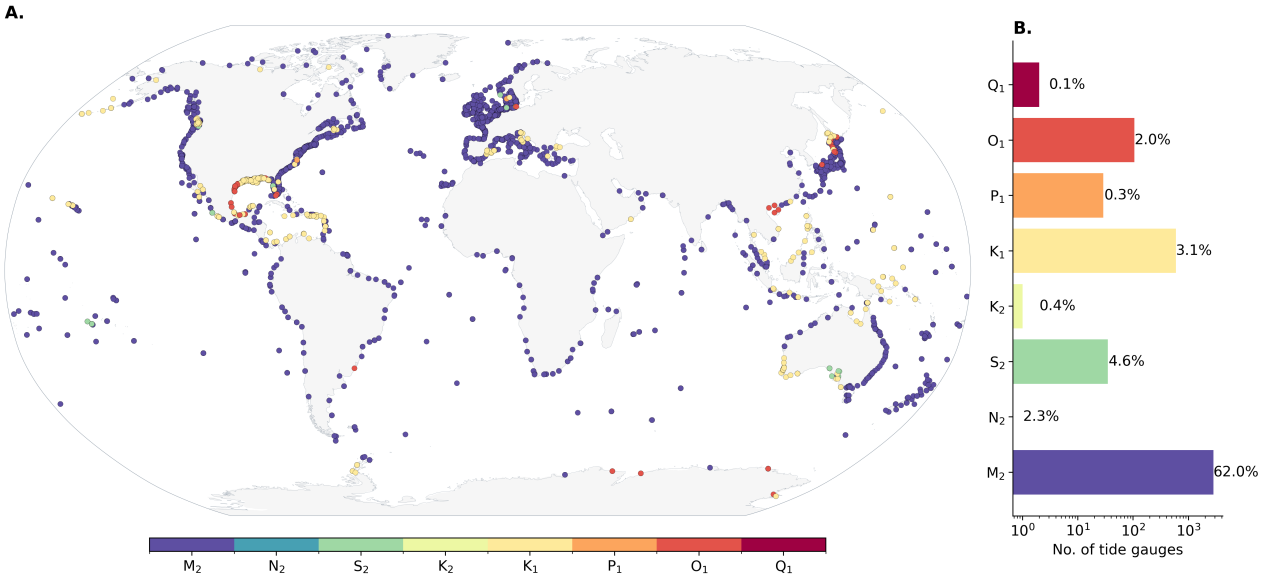

Figure 2. (A) The largest major constituent for each tide gauge as well as (B) the number of tide gauges where a constituent is the largest. The percentage numbers are the median explained percentage variance of each constituent.

amplitudes are typically relatively low, usually in the single millimeter range and rarely exceeding 1 cm, in TICON-4, we identify that the $^3N_2$ and $^3L_2$ constituents exceed 2 cm amplitudes at 20 tide gauges. The terdiurnal M_3 can be larger, exceeding 10 cm on some localized shelf resonances (Huthnance, 1980). Overall, a large number of the 33 constituents have amplitudes exceeding 2 cm across the numerous tide gauges (Figure 3B and 3D), with 23 of these constituents exceeding this threshold for more than 100 tide gauges. This further emphasises the importance of minor tidal constituents and of accounting for their contributions to tidal predictions, both directly from observations and within global tide models.

The long-period tides, with periods ranging from 1 week to 18.6 years, are not included in our analysis in Figure 3, allowing emphasis to be placed on the daily and sub-daily bands; however, their exclusion does not diminish their importance. These constituents (Sa, Ssa, Mm, Mf, Mt, etc.) are produced by various motions of the Sun and Moon that, in essence, modulate the forcing for the Earth's permanent tide. They are generally only a few cm or smaller. At many coastal gauges, MSf is inflated by nonlinear effects (its frequency equals the difference between S_2 and M_2 frequencies). The Sa constituent, however, is a "meteorological tide," driven by seasonal climatic effects associated primarily with the sun's annually varying declination. Owing to this strong forcing, the observed Sa is usually the largest of the long-period constituents (on average, about 7.6 cm); see Figure 6C below. The semiannual Ssa is also primarily meteorological, but it also has a significant gravitationally driven part (e.g., Ray et al., 2021). See also Ponte and Schindelegger (2024) for a more extensive discussion of these two long-period constituents as seen at coastal tide gauges.

https://doi.org/10.5194/egusphere-2026-346
Preprint. Discussion started: 4 February 2026

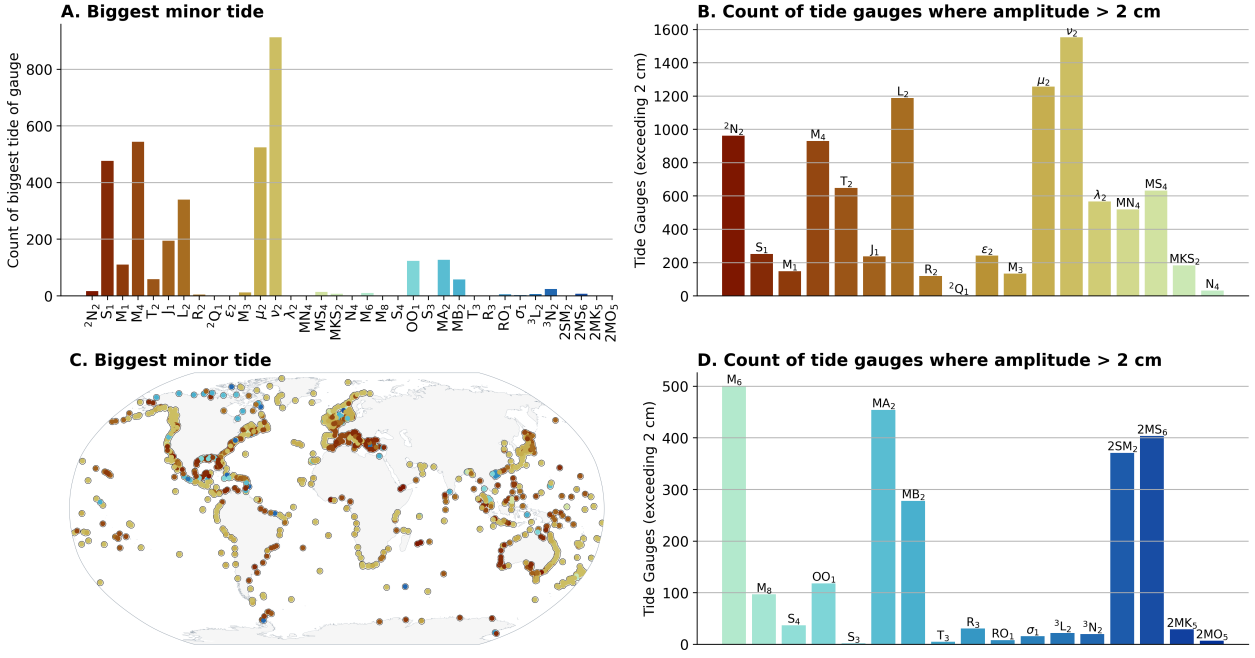

Figure 3. The largest minor tide and the number of gauges when a constituent exceeds a 2 cm amplitude.

4 Tidal Characteristics

Along large stretches of the world's coastlines, tides play a crucial role in coastal flooding events, either amplifying or dampening the effects of high-water events commonly caused by storm surges. The contribution of tides to coastal flooding largely depends on the tidal amplitude, or tidal range, which is defined as the height difference between successive low and high tides. Figure 4A displays the maximum tidal range. Tidal ranges differ greatly across global coastlines, from only a few cm in semi-enclosed seas such as the Mediterranean, the Baltic, and the Caribbean, to exceeding 10 m in macrotidal areas such as the Bay of Fundy, the English and Bristol Channels, the Patagonian Shelf, and northern Australia.

Naturally, the global distribution of HAT, MHW, and MHHW (Figure 5) is quite comparable to the maximum tidal range. A slightly altered pattern is displayed in Figure 5D, which shows MHHW-MHW, i.e., the average height difference of two consecutive high waters. Higher values are obtained for mixed tidal regimes with considerable amplitudes. Tide gauges are strongly influenced by diurnal and semi-diurnal tidal processes due to the forcing produced by the Moon and the Sun. However, depending on the tide gauge's position and location and the region's oceanographic characteristics, the relative contributions of semidiurnal and diurnal tides vary. Typically, tidal frequencies are categorized into different tidal regimes: long-period tides (lasting longer than 24 hours), diurnal tides, mixed tides, semi-diurnal tides, and short-period tides (with periods shorter than 12 hours). Several measures provide insights into which frequency band is most energetic. For example, the sum of tidal constituent amplitudes within each respective tidal band provides an approximation for which band contributes most to high

https://doi.org/10.5194/egusphere-2026-346
Preprint. Discussion started: 4 February 2026

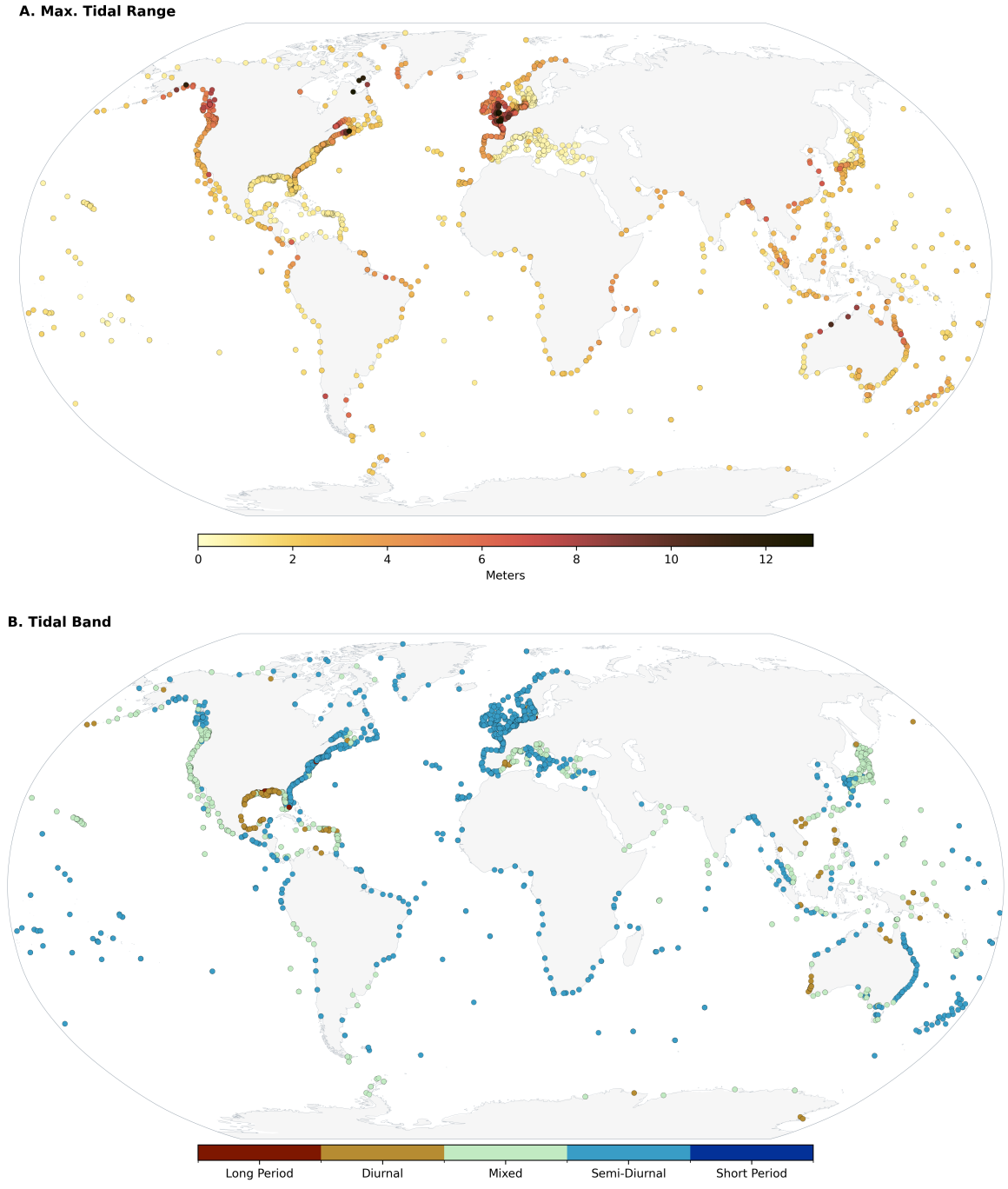

Figure 4. The tidal range and dominant tidal band for each tide gauge in GESLA-4. In Figure B1, examples are shown of tide gauges in each tidal band.

https://doi.org/10.5194/egusphere-2026-346
Preprint. Discussion started: 4 February 2026

and low water (Figure 4B). When the sum of the diurnal and semidiurnal amplitudes is within 50% of each other, water levels follow a 'mixed' tidal regime with a pronounced inequality in the roughly twice-daily high and low tides.

An additional measure that describes the relative contributions of diurnal and semidiurnal forcing is the tidal Form Factor (Figure 5A). The Form Factor (FF) is the ratio of the two major diurnal constituents (O_1 + K_1) to the two largest semidiurnal constituents (M_2 + S_2). For FF values lower than 0.25, tides are considered semi-diurnally dominant; for values between 0.25 and 1.5, tides are considered mixed semi-diurnal; for values between 1.5 and 3, tides are mixed diurnal; and for values exceeding 3, tides are considered diurnally dominant.

Complementary to FF, we next introduce a 'dodginess' parameter that describes the extent to which the apparent amplitude of the local tide varies over a lunar cycle. A significant reduction in this apparent amplitude can occur if the dominant partial tides (frequencies f_1 and f_2) of the respective tidal regime have nearly equal magnitudes. In this case, a tidal beat is created, with the beat frequency $(f_2 - f_1)/2$ modulating the amplitude. Often, the constituents at play are M_2 and S_2, as in the case of Port Adelaide situated in the Gulf Saint Vincent in South Australia, which is famous for its 'dodgy' tidal regime that tends to completely decay on a fortnightly period (e.g., De Ruyter, 2025). Since a 'dodgy' behavior is also possible in diurnal regimes, dominated by K_1 and O_1 (e.g., New Orleans), or mixed tidal regimes (e.g., the South coast of Borneo), we define the parameter 'dodginess' as:

$$\text{Dodginess} = 1 - \frac{|A_{K1} - A_{O1}| + |A_{M2} - A_{S2}|}{A_{K1} + A_{O1} + A_{M2} + A_{S2}} \tag{2}$$

Thus, a value of 1 quantifies a very dodgy tidal regime, while 0 signifies non-dodgy tides. While the parameter does not perfectly capture all possible conditions that produce dodgy tides, it provides a robust metric for estimating the abundance of tidal beating in the world's oceans, which is clearly dominated by the four utilised tides (Figure 2). Extended dodgy tidal regimes are indicated, e.g., for the Antarctic Coast, the Gulf of Mexico, South Australia, the Gulf of California and the adjacent Mexican West Coast, and parts of the Indonesian Archipelago (Figure 5F and B2). Further, local resonances cause concentrated dodgy tides, e.g., in the Gulf of Carpentaria and the Gulf of Gabes in Tunisia. The latter represents a curious exception to the generally microtidal Mediterranean Sea with a tidal range of up to 2 meters (Sammari et al., 2006). The vast majority of stations are dominated by tidal frequencies within the semi-diurnal range, with a geographical pattern similar to that of the largest major constituents, as shown in Figure 2 above. Despite this, there are regions driven by diurnal constituents, particularly the Gulf of Mexico and the southwestern coast of Australia. Long-period tidal constituents are typically smaller than those of the higher frequency constituents. In regions such as the Baltic Sea or Black Sea (which are excluded from our analysis), where the tidal range is considered negligible, these long-period constituents are often the dominant signal.

In the remainder of this section, we present a global analysis of several further statistics that help understand tidal dynamics, providing insights useful for a variety of biogeophysical studies, ranging from compound flooding mitigation to ecosystem functioning. In Figures 6A and 6B, the age of tide and the age of diurnal tide are presented. The age of the tide is an old, but still scientifically useful, term for the lag between the new or full Moon and the maximum spring tidal ranges. It arises from the ocean tide being unable to respond instantly to the tidal potential forcing but having to adapt to other forces, for example,

https://doi.org/10.5194/egusphere-2026-346
Preprint. Discussion started: 4 February 2026

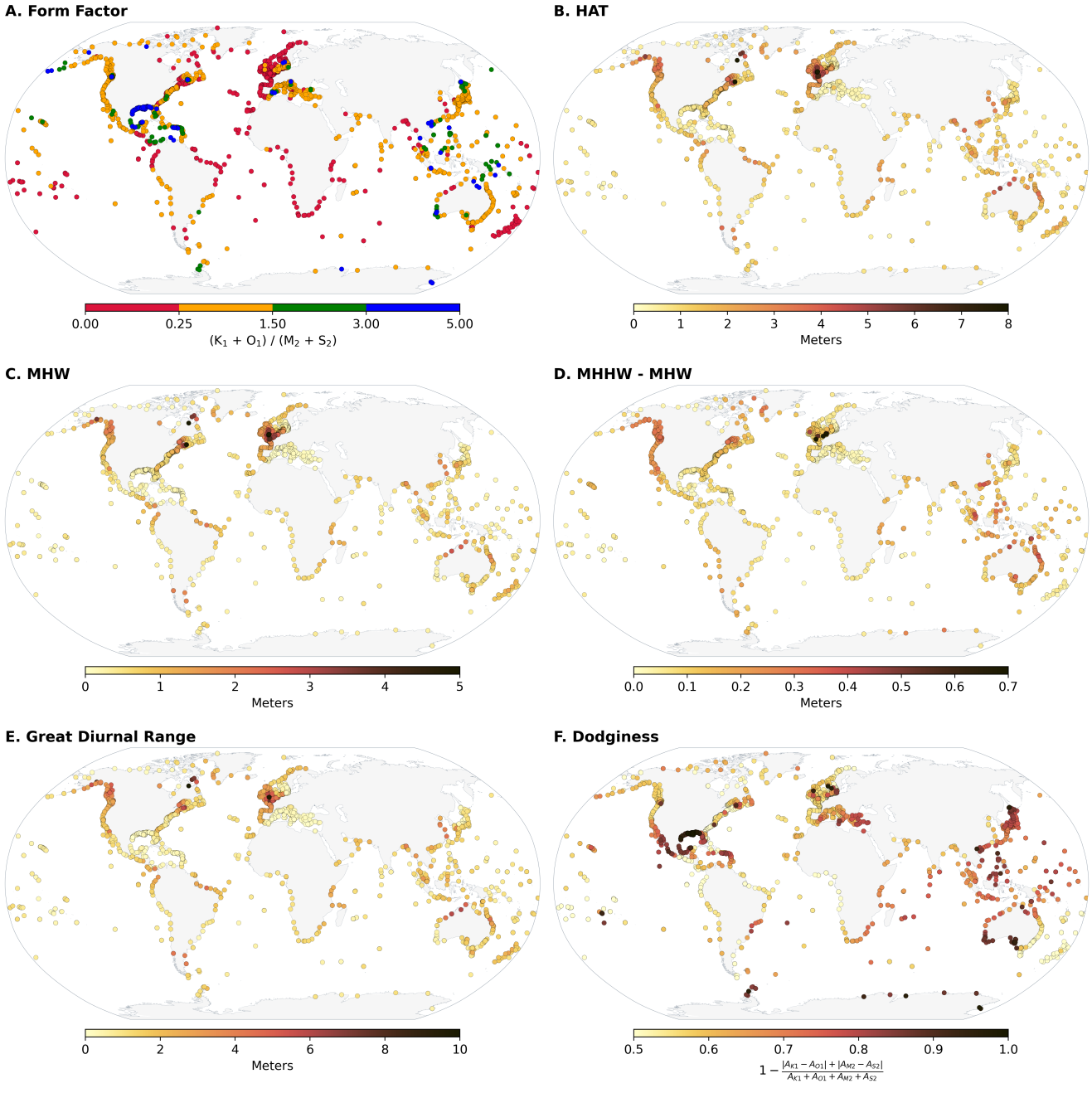

Figure 5. Form Factor, Highest Astronomical Tide (HAT), Mean High Water (MHW), Mean Higher High Water (MHHW), Great Diurnal Range, and Dodginess derived from each tide gauge.

https://doi.org/10.5194/egusphere-2026-346
Preprint. Discussion started: 4 February 2026

friction and to large-scale resonances of ocean basins, that contribute to its dynamics (Garrett and Munk, 1971; Webb, 1973) (The large-scale character of this parameter can be seen better in Figure B2).

The age of the semidiurnal tide at any one location is given by:

$$\text{Age of semidiurnal tide} = (G_{S2} - G_{M2})/(S_{S2} - S_{M2}) \tag{3}$$

where G_{S2} and G_{M2} are the Greenwich phase lags of the S_2 and M_2 constituents respectively. Alternatively, local phase lags, usually denoted by the Greek symbol κ, can be used for this calculation, where $\kappa = G + nL$, n being the species (2 in this case) and L the longitude east of Greenwich. S_{S2} and S_{M2} denote the speeds in degrees per solar hour of S_2 and M_2 (30 and 28.984 deg/hour, respectively). This lag (or age) typically has a positive value of several hours, though it varies by location. For example, it has a value of 18 hours in New York and 8 hours in San Francisco, but it is actually negative in Honolulu (Pugh and Woodworth, 2014). Liverpool's value is approximately 2 days, which is about the global average. In other words, the solar tides on average lag behind the solar tidal forces by a larger amount than the lunar tides lag behind the lunar forces (Doodson and Warburg, 1941). Previous maps of the age of the semidiurnal tide can be found in El-Sabh et al. (1987); Gil and De Toro (2005). Overall, the average positive age of the tide is a consequence of tidal dissipation. More concretely, one would expect larger tidal amplitudes only after the occurrence of a full Moon, since the full Moon is the cause for large tidal forces and, thus, amplitudes. Therefore, at a first glance, regions with a negative age of the tide, e.g., the Coral Sea (Webb, 1973), seem to contradict causality. However, this can be a consequence of the oceans' resonant nature, in which tidal energy is permanently redistributed, leading to a spatially and temporally localized concentration by interference that leaves causality untouched.

Similarly, an age for the diurnal tide can be computed, which is the interval in hours between the maximum declination of the Moon and the time of high water of the following (diurnal) spring tide (Doodson and Warburg, 1941). In harmonic terms, it can be represented by:

$$\text{Age of diurnal tide} = \frac{G_{K_1} - G_{O_1}}{S_{K_1} - S_{O_1}}. \tag{4}$$

where G_{K_1} and G_{O_1} are the Greenwich phase lags of the K_1 and O_1 constituents and S_{K_1} and S_{O_1} are their speeds. Previous maps of the world coastline for this quantity have been presented by El-Sabh and Murty (1989); values vary considerably spatially, with the largest (approximately 57 hours) in the Atlantic and the smallest (approximately 4 hours) in the Indian Ocean. It is probably true to say that this diurnal age parameter is made much less use of now in scientific studies than the semidiurnal age of the tide.

The lunitidal interval is the time between the transit of the Moon and the next high water at a particular location. It varies over the spring-neap cycle, with its average over the cycle called the Mean High Water Interval (MHWI) or 'corrected establishment'. Its value near the time of full and new Moon is called High Water Full and Change (HWFC) or 'vulgar establishment'. HWFC is larger than MHWI by about half an hour if the age of the tide is about 2 days, as is the case for many locations around the world. These quantities seem somewhat archaic nowadays, but in the days of sailing ships, captains would have been intimately familiar with HWFC values for each coastline they operated along. For example, Captain James Cook was able to compile short tables of tidal range and HWFC at locations he visited during his voyages of discovery (Woodworth and

https://doi.org/10.5194/egusphere-2026-346
Preprint. Discussion started: 4 February 2026

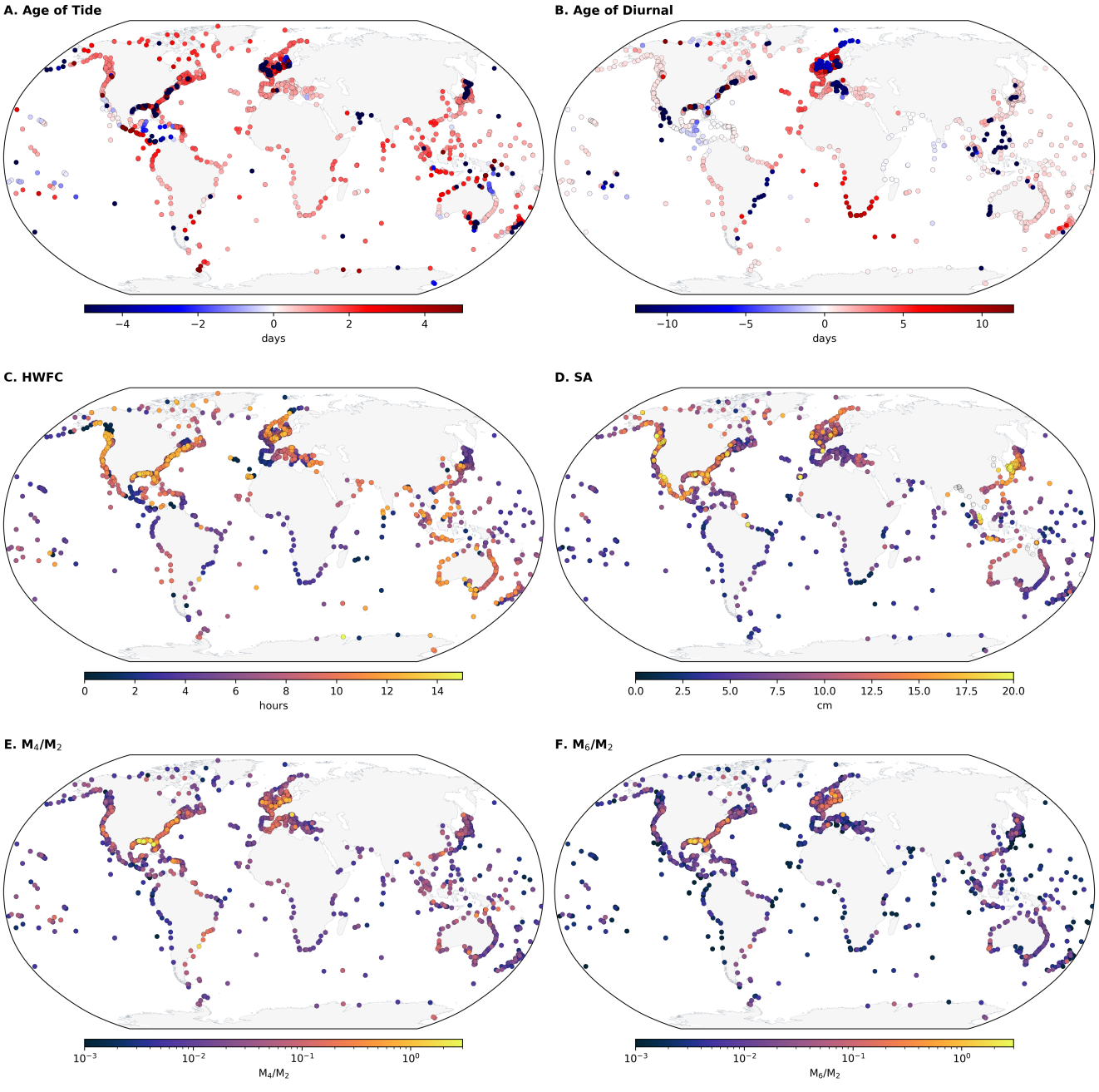

Figure 6. Age of Tide, Age of Diurnal tide, HWFC, Solar Annual (Sa) constituent, ratio of M_4/M_2, and ratio of M_6/M_2. A selection of these results is shown for the FES2022 model in Figure B2.

https://doi.org/10.5194/egusphere-2026-346
Preprint. Discussion started: 4 February 2026

Rowe, 2018). In practice, one has to be careful with the term 'establishment', HWFC itself being referred to as 'establishment' by Lubbock (1831), and subsequently as 'vulgar' or 'common establishment' by Whewell (1833). Cartwright (1999) gives a history of how Lubbock and Whewell came to use these terms. For present purposes, we have taken it to be HWFC as shown in Doodson and Warburg (1941) and Appendix A of Woodworth and Rowe (2018).

In Section 3, we briefly mentioned some nonlinear constituents, which are typically generated in shallow water as the progression of a tidal wave is modified by bottom friction, coastline geometry, and river dynamics. Locally, weather-induced extreme water levels may interact with the tidal signal. Increased water depth during a storm surge modifies the tidal phase speed, such that it arrives before the predicted tide (Horsburgh and Wilson, 2007).

Additionally, frictional interactions between the tidal and surge currents extract energy from both waves (Familkhalili et al., 2020). Thus, tide-surge interaction modifies both the magnitude of the sea level extremes and the timing of the peak, with extremes occurring preferentially during the rising tide (e.g., Horsburgh and Wilson, 2007; Idier et al., 2012). These interactions are more remarkable in areas with large tidal ranges and over wide continental shelves. In regions dominated by the semi-diurnal tidal constituents, one can frequently investigate the ratios of the amplitudes of M_4 and M_6 tides with respect to M_2, which gives insight into whether a gauge or location is influenced by tidal asymmetry. In Figures 6E and 6F, these ratios are presented, with higher values indicating a stronger influence on nonlinear effects. However, this approach is only representative when the amplitude of M_2 is significant.

Contrasting these findings with those of directly measured shallow water constituents, such as those observed in Figure B3, we can isolate regions especially influenced by shallow water constituents: the North Sea, Gulf of Alaska, the Patagonian shelf, several locations in South East Asia, and the northwestern Australian coastline. Within the North Sea, these nonlinear effects have been well-studied and modelled (Pingree et al., 1984), and are caused by the interactions of large tidal waves with the shallow bathymetry in the region. Results in the Gulf of Mexico also indicate larger nonlinear influences from the ratios shown in Figures 6E and 6F, but contain a relatively smaller tidal range and less influence from the semi-diurnal tidal constituents. A complementary tidal statistic to this analysis is whether the superposition of semidiurnal and diurnal constituents tends to produce especially large high waters or is more biased toward low outliers; readers are referred to the discussion by Byun et al. (2023) for more information on this.

5 Tidal duration

The duration of each high-water and low-water period depends on its magnitude and shape, both of which vary depending on a constantly shifting superposition of sine waves caused by the major and minor constituents and their phases (Talke, 2025). Thus, two tides with the same peak water level may spend a different amount of time within 1 or 20 cm of the peak, due to variations in shape. Globally, we evaluate the top thirty high tides in a year of tidal predictions to derive the median duration of these peaks within particular thresholds. In Figure 7, only records with minimal river influence and tidal ranges greater than 15 cm are considered (see Talke, 2025, for additional discussion of the Methods). Regions with small, diurnal tides such as the Gulf of Mexico, exhibit spring high-tides of long durations, even for a small exceedance of 1 cm (Figure 7). By contrast,

https://doi.org/10.5194/egusphere-2026-346
Preprint. Discussion started: 4 February 2026

semidiurnal regions with large tidal amplitudes see Figure 5, such as the North Sea, the west coast of Norway, and the east coast of Brazil, exhibit much shorter durations near their peak high tide (Figure 7). Regions with large, mixed high tides, such as the Gulf of Alaska, are also marked by relatively short high-water stands. As tides become more diurnal in the western Aleutian Islands (Figure 5), the duration near the peak increases. Large durations near the peak are also observed in the Mediterranean, at islands in the Pacific Ocean, in the Arctic Ocean, and other locations with small amplitude tides. Around Australia, the diurnally dominant southwest experiences much longer high-water stands than the semi-diurnally dominant northwest, with the mixed-tides east coast somewhere in between. An order-of-magnitude variation in timescales is observed in Southeast Asia, particularly around the Japanese coast of the Sea of Japan (see Figure B4 for more details).

Globally, the coastal tides evaluated stay within 1 cm of their peak from 0.2 to 3.5 hours, with a mean of 1.0 hours. The time spent within 20 cm of the peak varies from 1 to 14 hours, with a mean of 4.7 hours. The duration near the peak matters for multiple reasons; for example, in regions subject to long high-water stands, waves may erode vulnerable shorelines for longer periods during storms. Additionally, tidal properties interact with storm surge to produce a composite wave; generally speaking, the longer the high-water stand, the longer the ensuing high-water period during a storm may be, given equal meteorological forcing. Ecological processes are often critically dependent on time out of water (emersion time) or time inundated. We note that the duration of mean tides, neap tides, and low-water periods may differ from the patterns shown in Figure 7, and that some variability in tide duration (generally <10%) will occur even between spring tides of the same magnitude, at a given location (Talke, 2025). This occurs because the mix of diurnal and semidiurnal tidal forcing, along with their phases, continually shifts. As shown in Talke (2025), the high or low water period that results can usually be represented as a sine wave with an amplitude and a period that is somewhere in between the main tidal bands. The resulting duration for a given inundation depth is directly proportional to this period.

6 Tidal changes

It is well understood that tidal characteristics have changed over long geological time scales, driven by tectonic processes (which alter the size, depth, and shape of the ocean which in turn impacts tidal propagation and resonance) and changes in Earth's rotation (tidal friction gradually slows Earth's rotation, lengthening the day and modifying the tidal frequencies and their resonance with ocean basins). However, over much shorter time periods of the last few hundred years, and perhaps because of the reliability of tide predictions, casual observers often assume that tidal constituents are stationary, because planetary orbital motions are stable and predictable. Nonetheless, it has been observed that tidal levels in many locations change considerably due to non-astronomical factors over seasonal, decadal, and secular time scales (Doodson, 1924). In their comprehensive review, Haigh et al. (2020) synthesise global evidence that tides are changing due to non-astronomical factors, documenting widespread regional trends in tidal amplitudes and constituent behaviour across the 19th to early 21st centuries (see also the review of Talke and Jay, 2020). They identify six principal local-scale drivers (such as bathymetric change, river discharge, and anthropogenic alteration) and eight broader regional/global mechanisms (including sea-level rise, ice-sheet collapse, and ocean stratification) that influence tidal variability. While attribution is challenging because coastal tidal signals reflect the integrated

https://doi.org/10.5194/egusphere-2026-346
Preprint. Discussion started: 4 February 2026

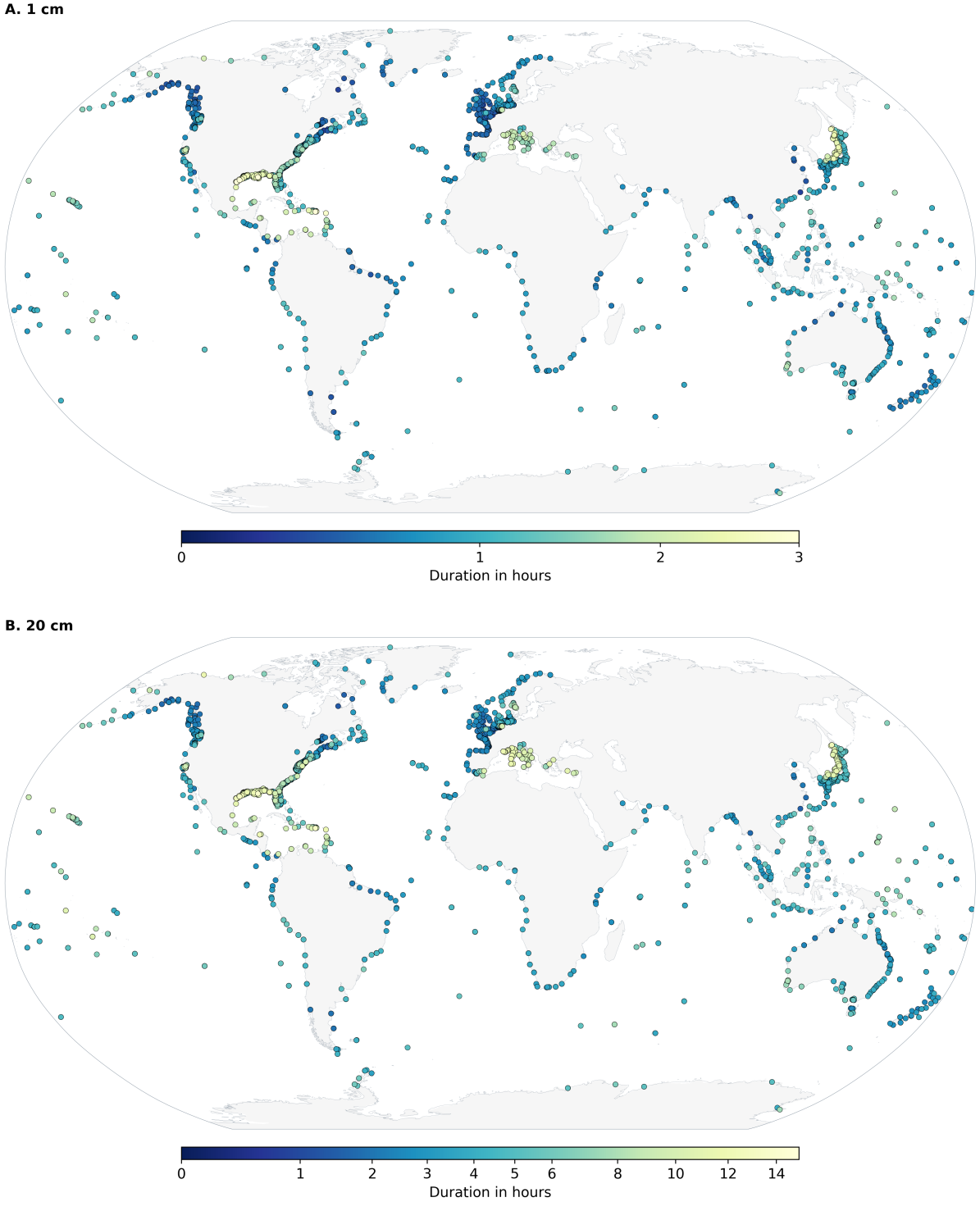

Figure 7. Water level duration within 1 cm (A) and 20 cm (B) thresholds from high tide. Some region plots are shown in Figures B4 and B5.

https://doi.org/10.5194/egusphere-2026-346
Preprint. Discussion started: 4 February 2026

effects of local, regional, and ocean-basin-scale influences, modelling studies reviewed indicate that future sea-level rise and changes in coastal morphology will continue to alter tidal regimes, with significant implications for coastal hazard assessment, ecosystem change, and infrastructure design.

To evaluate tidal changes observed from tide gauges, we calculated yearly amplitudes of the M_2 and S_2 tidal constituents and derived a trend relative to the TICON-4 amplitude estimations. This analysis focuses solely on gauges with more than thirty years of observations from the UHSLC research-quality (UHSLC-RQ) database, resulting in a total of 237 tide gauges. The thirty-year threshold is selected to minimize any correlation with possible non-equilibrium nodal modulations that are known to occur at some gauges (Feng et al., 2015). The results are shown in Figure 8.

Our analysis found that for both constituents, 52% and 53% of tide gauges showed a statistically significant (defined as when the amplitude trend exceeds the estimated uncertainty) trend for the M_2 and S_2 tide, respectively. For the M_2 tide, the trends are positive in 58% of the tide gauges, with mean absolute trend being 0.19 mm/year and ranging from -1.47 mm/year to 1.80 mm/year. For the S_2 tide, the trends are positive in 54% of tide gauges, with mean trending being 0.10 mm/year, ranging between -1.17 mm/yr to 0.98 mm/yr.

Tidal trends can be observed in both constituents, with their directions varying regionally. It is expected that the observed trends between M_2 and S_2 would be different due to their different astronomical forcings: roughly 15% of S_2 is radiational (Arbic, 2005). Of the 378 gauges, 62.4% of tide gauges exhibit consistent trend directions between the M_2 and S_2 amplitudes. In several regions, such as South Africa and the east and western coasts of America, these trends are largely coherent or consistent, but it can be observed that certain tide gauges do not conform to the trends expressed by nearby gauges, e.g. in the Gulf of Mexico and Japanese tide gauges. Such anomalous trends can result from a variety of factors, ranging from changes in tide gauge measurements, undocumented errors, or the influence of river processes on measurements (Woodworth, 2010).

Taking this into consideration, some regional conclusions can be drawn. For the S_2 tide, clear region-specific changes in the tides can be observed, particularly positive trends on the west coast of America and negative trends on the eastern coast, which agrees with the earlier findings (Jay, 2009; Ray, 2009; Woodworth, 2010). Our analysis shows that tide gauges in Southern Africa exhibit the largest variations in tidal amplitudes across both the M_2 and S_2 tides (Figure 8), particularly for long-term gauges located in harbours or estuaries (the Knysna tide gauge, located in an estuary in South Africa, exhibits the largest calculated M_2 trend, 1.80mm/yr), where tidal statistics measurements are susceptible to local changes dredging, land reclamation, and other geometric changes (Haigh et al., 2020; Talke and Jay, 2020).

7 A note on river tides

Tides in rivers, deltas, and estuaries are greatly influenced by river flow, geometry, and shallow water effects (e.g., Le Provost, 1991; Kästner et al., 2019; Talke and Jay, 2020). River flow causes enhanced friction on a tide wave, because bed stress depends on $|u|u$, where u is the sum of river and tidal flow (e.g., Dronkers, 1964; Godin, 1991; Kukulka and Jay, 2003; Kästner et al., 2019). In addition, tidal mass conservation induces non-linear effects when tidal range is comparable to the mean river depth. Thus, ocean constituents such as M_2 decrease in the upper river sections, while overtides such as M_4 often amplify, as river

https://doi.org/10.5194/egusphere-2026-346
Preprint. Discussion started: 4 February 2026

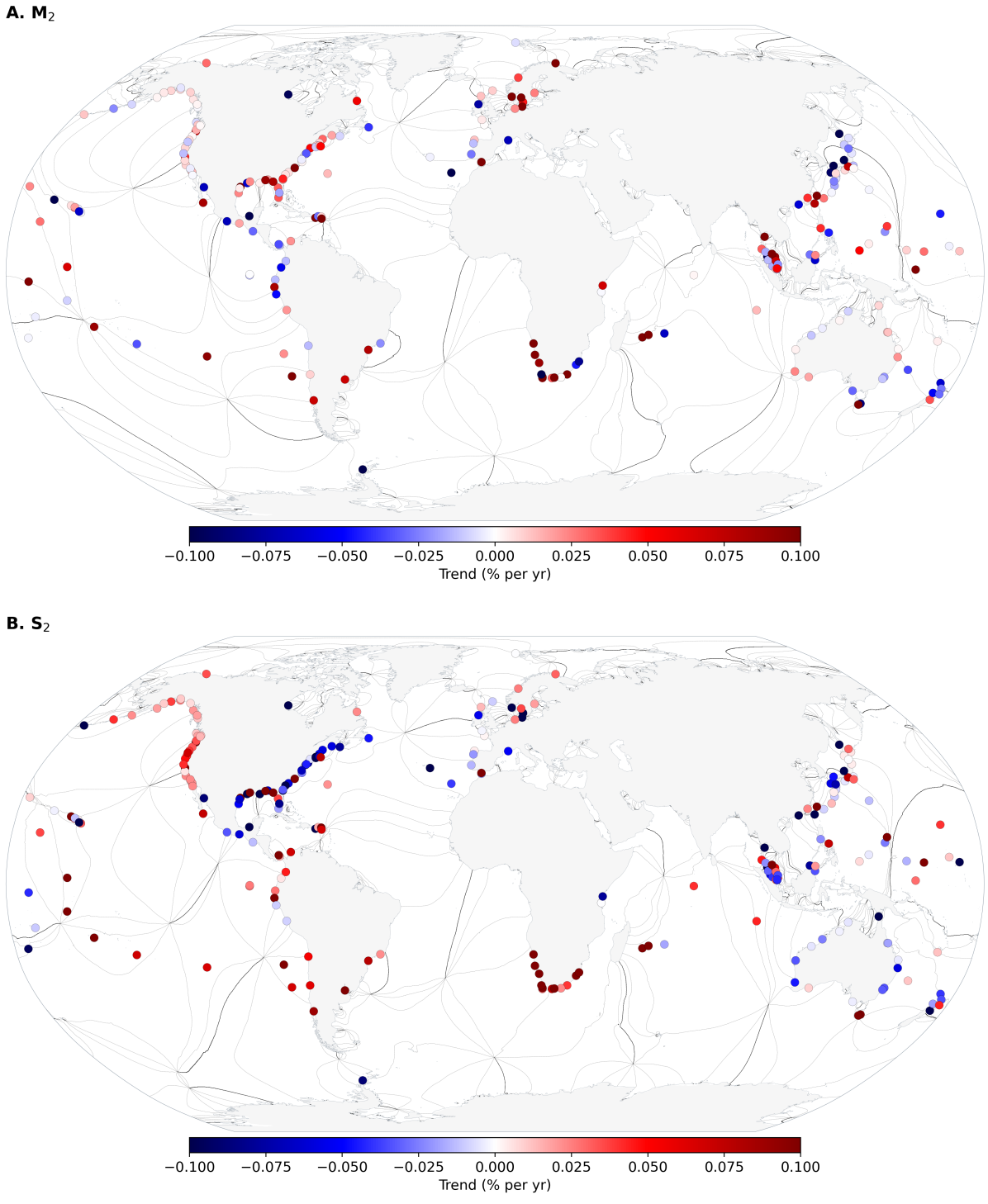

Figure 8. M_2 and S_2 amplitude percentage trend derived from UHSLC research quality tide gauges with at least 30 years of observations. The black contour lines are the phase lag of the respective constituents obtained from FES2022.

https://doi.org/10.5194/egusphere-2026-346
Preprint. Discussion started: 4 February 2026

flow increases (our analysis of the river tide gauges showed that the 'minor' tides exceed the major tides in about 50.5% of river tide gauges). This observation was used by Moftakhari et al. (2013) to estimate river flow from the San Francisco tide gauge during periods when no river discharge measurements were available. As tidal constituents such as M_2 decrease, river flow causes mean (e.g., tidally averaged) water levels to rise (e.g., Kästner et al., 2019; Talke et al., 2021). Thus, tidal datums are a function of river flow; a combination of decreased tidal range and increased mean water levels means that MLLW increases faster than MHHW when river flow increases (e.g., Jay et al., 2011).

The influence of river flow on tides tends to increase further upstream, both because effects are cumulative but also because river velocities are larger upstream, due to smaller width and depth; far enough upstream, the current never reverses, though tides continue to propagate upstream until they either dissipate (e.g., >500 km in Amazon River; Coulet et al., 2025) or reflect off a natural or constructed dam (e.g., Ralston et al., 2019). River-modulated friction effects influence spring tidal range more than neap tides (e.g., Buschman et al., 2009), and increase the mean river surface slope more (e.g., Kukulka and Jay, 2003); thus, far enough upstream, neap tides may produce lower water levels than spring tides (Jay et al., 2015; Hoitink and Jay, 2016). These characteristics of river tides, i.e., the transition point to lower neaps, the point of no reversal, and the location of upstream disappearance (for dam-less rivers), shift downstream (generally) as river discharge increases. All these non-stationary properties pose a challenge for evaluating tides using satellite-based measurements since the measurement frequency is often much smaller than the scales of river flow variability, and the strength of non-linear interactions also depends on natural shifts in astronomical forcing. Encouraging findings using the SWOT satellite to measure tides within rivers, has opened the door to investigating the tidal characteristics and tidal extent within rivers using harmonic analysis (Hart-Davis et al., 2026), which may benefit future analysis in studying the spatial variability of tides within rivers and assess the role of non-stationary components on the tidal dynamics, using approaches such as NS_{Tide} or a wavelet-based approach like CWT_{Multi} (Matte et al., 2013; Lobo et al., 2024).

The propagation speed of a tidal wave is also influenced by river flow. Most obviously, increases in depth caused by discharge increase the inviscid wave celerity ($\sqrt{g.h}$, where h is depth). Less obviously, the enhanced friction caused by river flow reduces wave celerity, counteracting increased depth (e.g., Parker, 1991; Jay, 1991). The frictional effect on celerity caused by river flow is a function of wave frequency, with lower frequency waves being less affected; thus, the phase speed of diurnal waves may differ from semidiurnal waves, also because they are influenced differently by convergent geometry (Jay, 1991). Depending on geometry, tide wave propagation speeds can be accelerated or slowed, in a way that depends on frequency and the amount of friction; in a convergent, funnel-shaped estuary, some wave frequencies act as an inviscid standing wave (infinite phase speed), while others are more strongly frictional (see e.g., Dykstra et al., 2024). Thus, a dispersion of long waves occurs (to some extent) in estuaries and rivers, modulated to some extent by river currents, with implications for shape and duration. The extraction of energy to overtides also tends to make tidal waves more asymmetric in rivers, influencing the duration of the high and low-water stands; far enough upstream, tides often become flood-dominant, with a short, steep flood period and a longer, more gentle ebb. The transition to flood tide at low water is typically much more abrupt than the ebb transition in such channels.

https://doi.org/10.5194/egusphere-2026-346
Preprint. Discussion started: 4 February 2026

Frictional interaction between tidal constituent pairs (e.g., S_2-M_2), triads (K_1-O_1-M_2), and river flow and constituents also contributes to different attenuation rates of the major constituents in an estuary and river. Phases of waves may also be shifted by the addition of overtide energy to a major constituent; for example, K_2 is an overtide of K_1, and M_2 can be formed by the interaction of K_1 and O_1. The complex transformations of tidal constituents and the differences in phase speeds can produce a factor of 2x or more variation in the duration that a tide remains near its peak in an individual estuary, for the same tide (Talke, 2025). Finally, the interaction of tides with river flow also tends to produce longer-period, quasi-2-week fluctuations in water level that can propagate far upstream of the head of (diurnal and semidiurnal) tides. These fluctuations can be understood as a type of tidal pumping, in which more water is pumped into an estuary during the flood tide period than exits during an ebb (a Stokes-drift-like mechanism).

8 Concluding remarks

This study has focused on evaluating tides from tide gauge records, which has been made possible by the multiple efforts to provide sustained and consistent datasets of sea level from providers such as GESLA and UHSLC. The continued efforts to maintain these high-quality datasets are crucial not only for tidal research but also in the study of long-term sea level and flooding events. It is quite clear that in parts of the global coast, there are significant gaps in observations, particularly in the global South. While some of this may be due to governmental restrictions, a significant portion of the issue stems from the lack of capacity and finances to not only deploy but also maintain tide gauges.

Although satellite observations provide suitable coverage of ocean tides, it is essential to emphasize that tidal research relies on tide gauge observations to continue our understanding of tidal variability across the global oceans. They complement altimetry by providing invaluable “ground truth”, by allowing assessments of long-term changes, and by revealing fine-scale details of the tidal spectrum.

Further gaps are evident in the polar coastal oceans, largely due to the challenges of maintaining measurement equipment in these regions, which are characterized by harsh environments and remoteness. Global navigation satellite systems (GNSS) reflectometry is a new evolving technology for measuring sea level which has a huge potential in polar regions (Larson et al., 2013). The strengths are mainly that the infrastructure consisting of the GNSS and coastal continuously operating reference stations (CORS) may be re-used as a remote sensing technique. No additional equipment mounted in the water is required, which is especially beneficial in harsh environments. Efforts are ongoing to explore the incorporation of GNSS reflectometry in tidal research, particularly in the polar regions (Tabibi et al., 2020), which will help provide further coverage in the future.

Ocean bottom pressure sensors are important sources of in-situ measurements of tidal characteristics in the global oceans (Ray, 2013), providing greater coverage, including in higher latitudes (Hart-Davis et al., 2024). However, globally available datasets of GNSS-R and ocean bottom pressure sensors applicable for such an analysis, as presented in this study from GESLA-4, do not currently exist. As these measurements continue to be collected, a public archive of these data will be useful for further investigating ocean tides on a global scale. Finally, there are still a large number of sea level records available around the world in paper-based format (Talke and Jay, 2013; Talke et al., 2013; Pouvreau, 2008; Bradshaw et al., 2015; Latapy et al., 2023). Finding and digitising these records, however, remains a difficult and time-consuming endeavor.

https://doi.org/10.5194/egusphere-2026-346
Preprint. Discussion started: 4 February 2026

Data availability. The TICON-4 dataset is available at https://doi.org/10.17882/109129 (Hart-Davis et al., 2025), while GESLA-4 is available at www.gesla.org (Haigh et al., 2026). An interactive map showing aspects of the TICON-4 is available at: https://openadb.dgfi.tum.de/en/tidal-constituents/map/. The FES2022 model can be obtained at: https://doi.org/10.24400/527896/A01-2024.004 (Lyard et al., 2021, updated). The trend, high tide duration, and tidal characteristics calculated in Figures 5 and 6 are available at: https://doi.org/10.17882/111620.

Code availability. The code to replicate the tidal prediction is available at https://www.tugraz.at/institute/ifg/downloads/ocean-tides.

https://doi.org/10.5194/egusphere-2026-346
Preprint. Discussion started: 4 February 2026

Appendix A

To construct the admittance matrix used for tidal inference, we assume a linear admittance based on several pivot tides from TICON-4. We exclude tides that have a significant radiational component (e.g., S_1, S_2, R_3, ..) as pivot tides. Admittance is separately applied for degree-3 tides contained in TICON-4 ($^3N_2$, $^3L_2$, M_3) which implicitly estimate 9 tides from Hartmann and Wenzel (1995), increasing the total number of tides to $M = 159$ (Figure A1) Further, the tide-raising forces are explicitly corrected for the FCN-resonance that disturbs the tide-raising forces for the K_1 tidal group. Based on the admittance matrix, tidal heights are computed according to the formula

$$\text{Tide} = \sum_{i=1}^{N} \left(\sum_{j=1}^{M} A_{ij} \cos[\omega_j t + V_j] \right) H_i \cos(G_i) + \sum_{i=1}^{N} \left(\sum_{j=1}^{M} A_{ij} \sin[\omega_j t + V_j] \right) H_i \sin(G_i) \tag{1}$$

A numerical advantage of this formula is that the computation of the sum over j is independent of the respective tidal constituents, i.e., it has to be only computed once for all tide gauges. Furthermore, the construction A_{ij} can be easily tailored to the desired level of accuracy, ranging from using a unit matrix to lowering the threshold to an arbitrarily low level. Additional information, including examples of admittance matrices for satellite gravimetry and software for computation, can be obtained from https://www.tugraz.at/institute/ifg/downloads/ocean-tides.

To evaluate this approach with a more commonly used method, we compared tidal heights predicted from the perth5 software (Ray, 2025, https://codeberg.org/rray/perth5) and present differences between them for the large tide observed at the Brest tide gauge; see Figure A2. The total variance difference between these two approaches is 1.91 cm^2 (median difference of 1.22 cm), a small fraction of the signal variance at Brest, which is approximately 25000 cm^2.

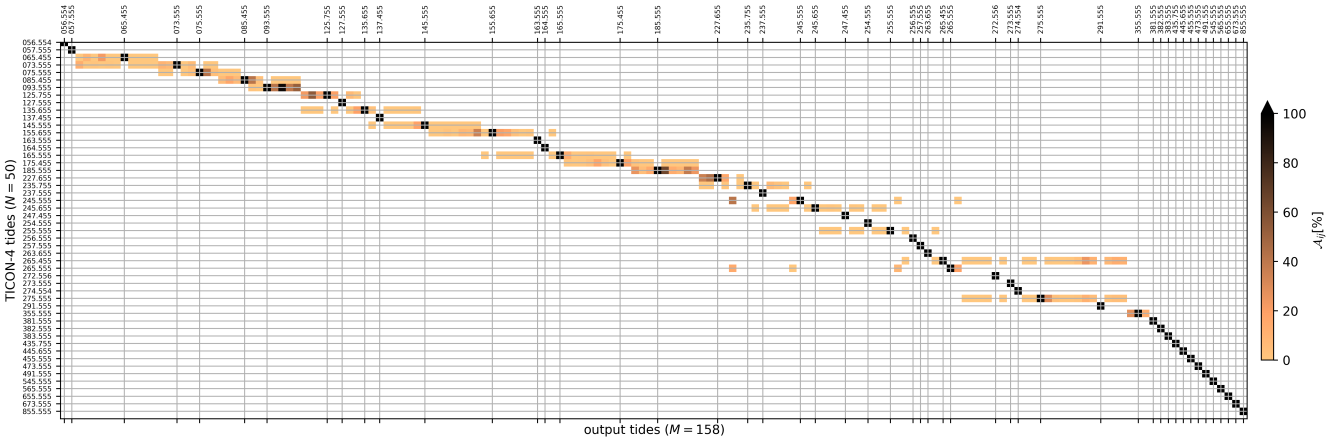

Figure A1. Admittance matrix employed within this study in %. The section describing degree-3 admittance (red) is marked out. Radiationally-contaminated tides and shallow-water tides are disallowed as pivot tides (e.g., S_1: 165.55 and M_4: 455.555). TICON-4 tides are labeled with their Doodson codes on the input and output sides of the matrix.

https://doi.org/10.5194/egusphere-2026-346
Preprint. Discussion started: 4 February 2026

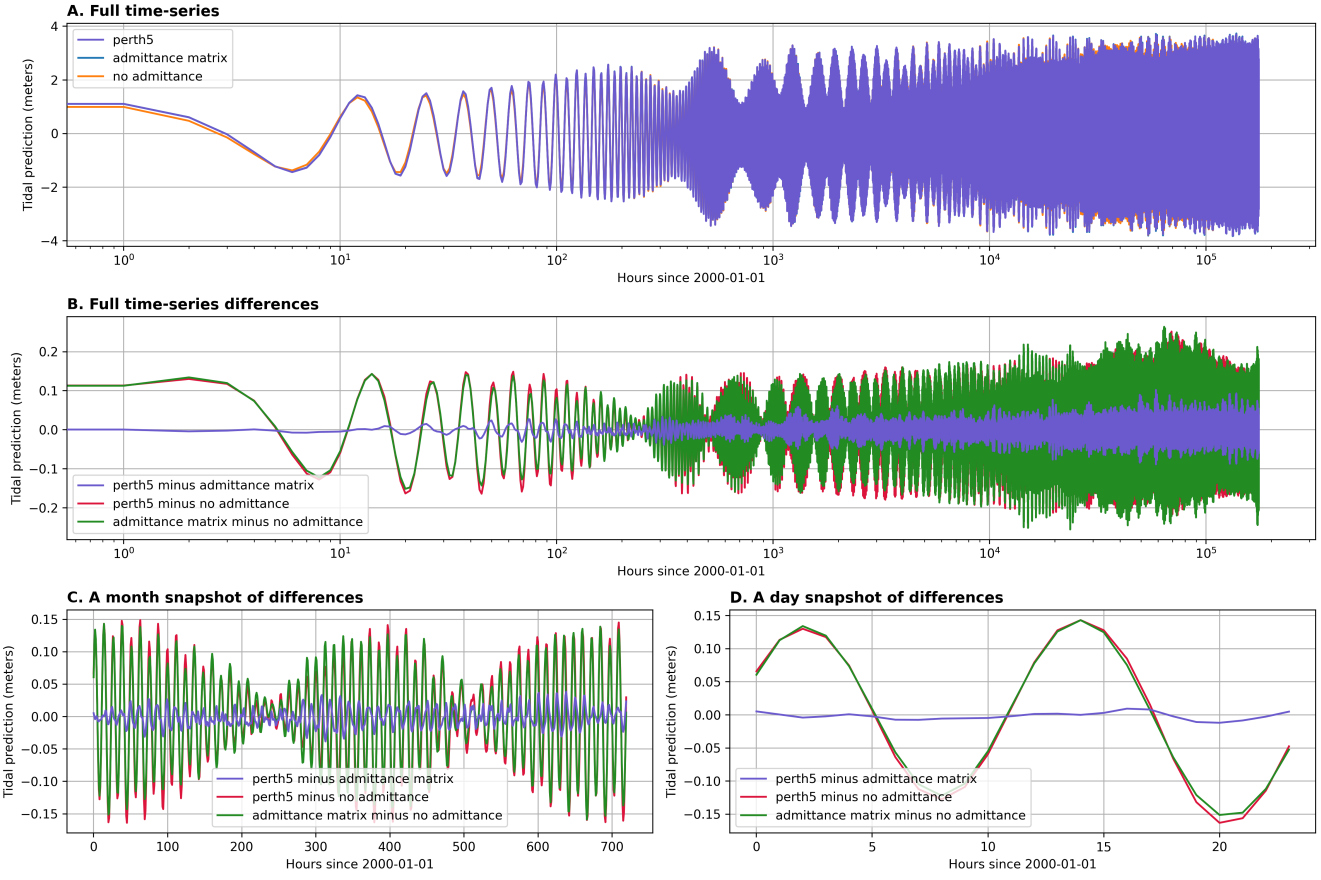

Figure A2. Comparison of tidal predictions made by the methods presented in Appendix A with and without admittance, and the perth5.f software. (A) presents a 20-year prediction by the three methods, with differences between the methods across the full time-series (B) as well as a month (C) and day (D) snapshot also shown.

https://doi.org/10.5194/egusphere-2026-346
Preprint. Discussion started: 4 February 2026

Appendix B

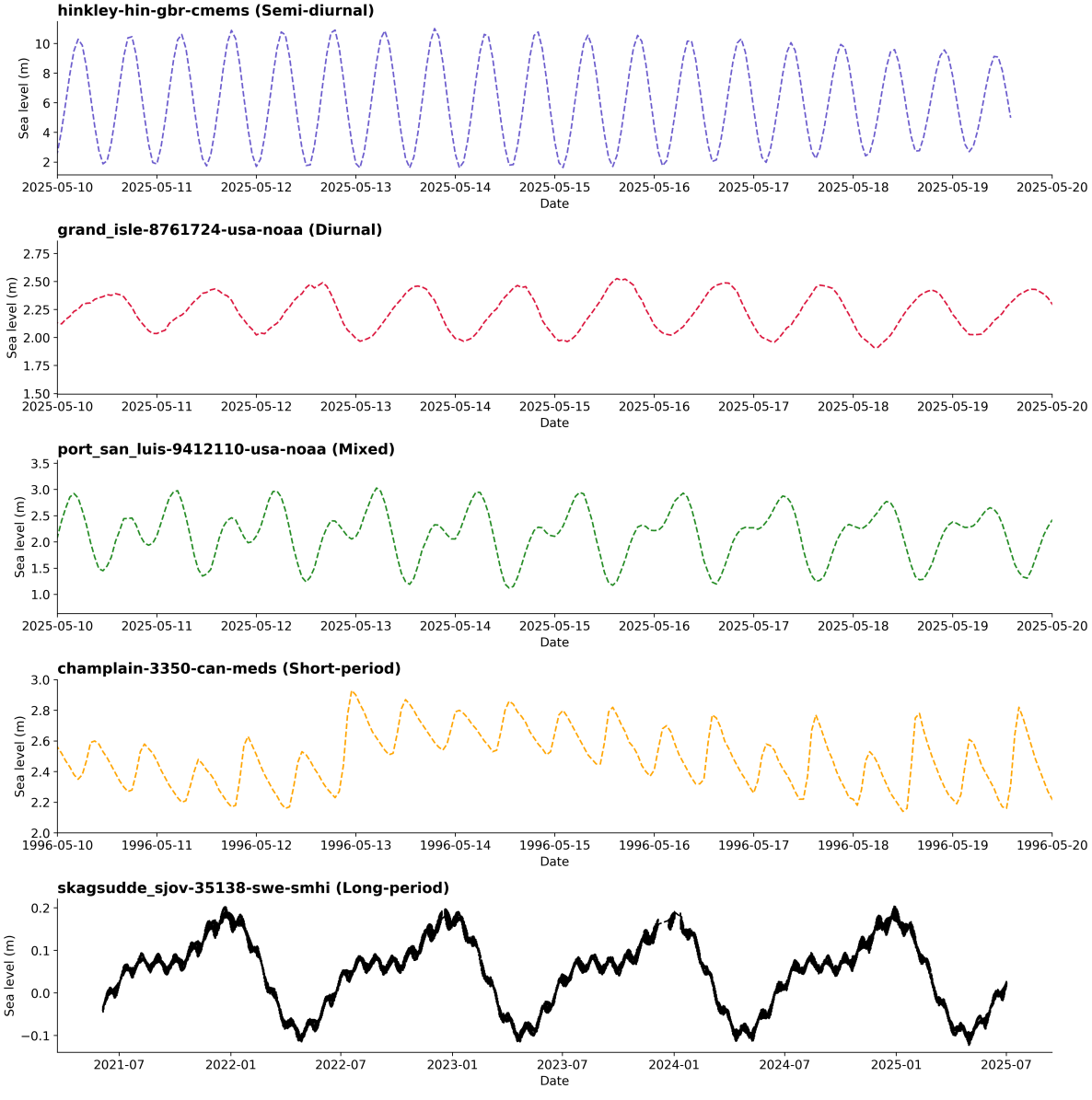

Figure B1. Time series of tide gauge data within each tidal band, as discussed in Figure 4. For the long-period example, non-tidal variability has been removed to highlight only the tidal contributions.

https://doi.org/10.5194/egusphere-2026-346
Preprint. Discussion started: 4 February 2026

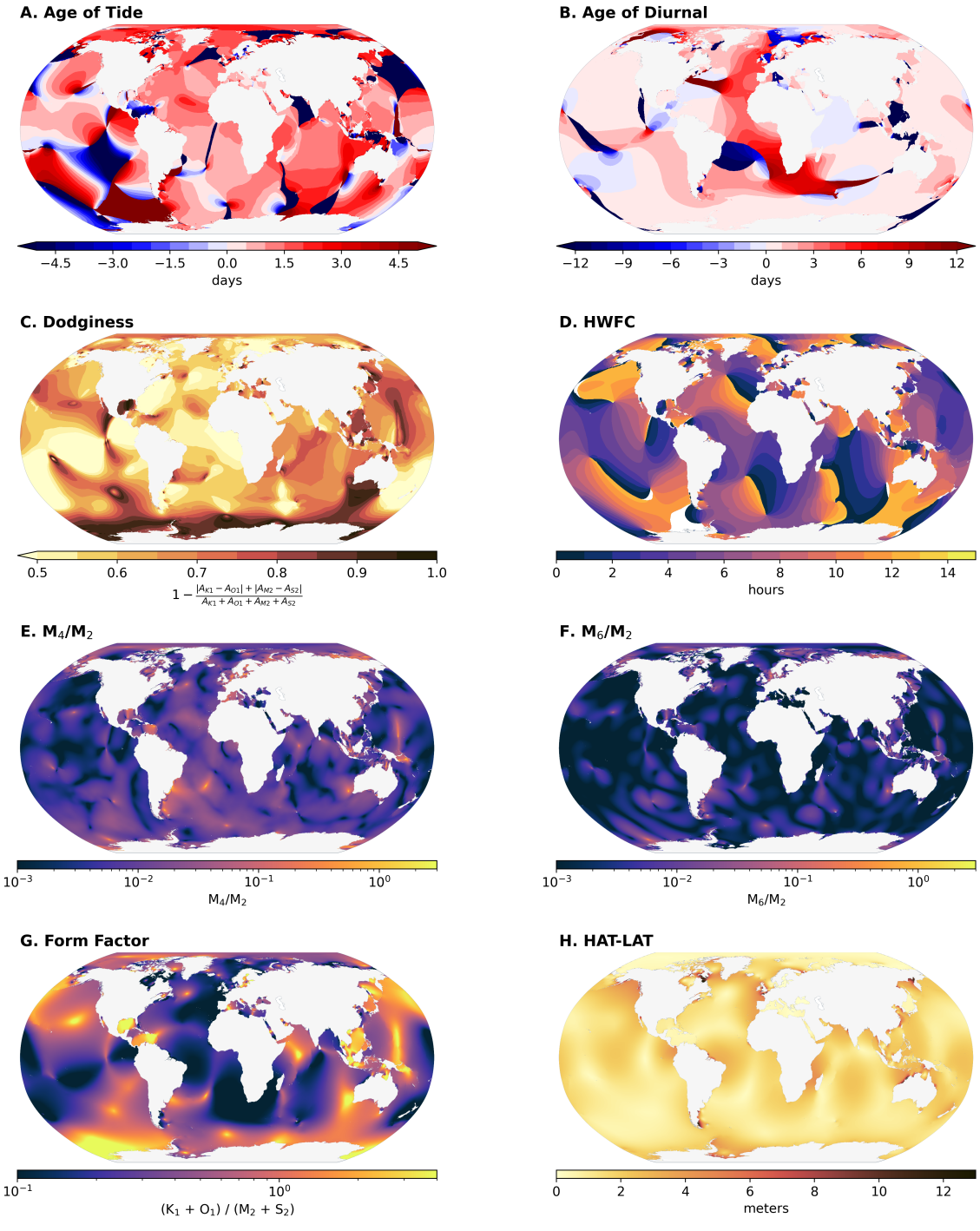

Figure B2. For comparisons to the results seen in the tide gauges, model results derived using FES2022 Lyard et al. (2021, updated).

https://doi.org/10.5194/egusphere-2026-346
Preprint. Discussion started: 4 February 2026

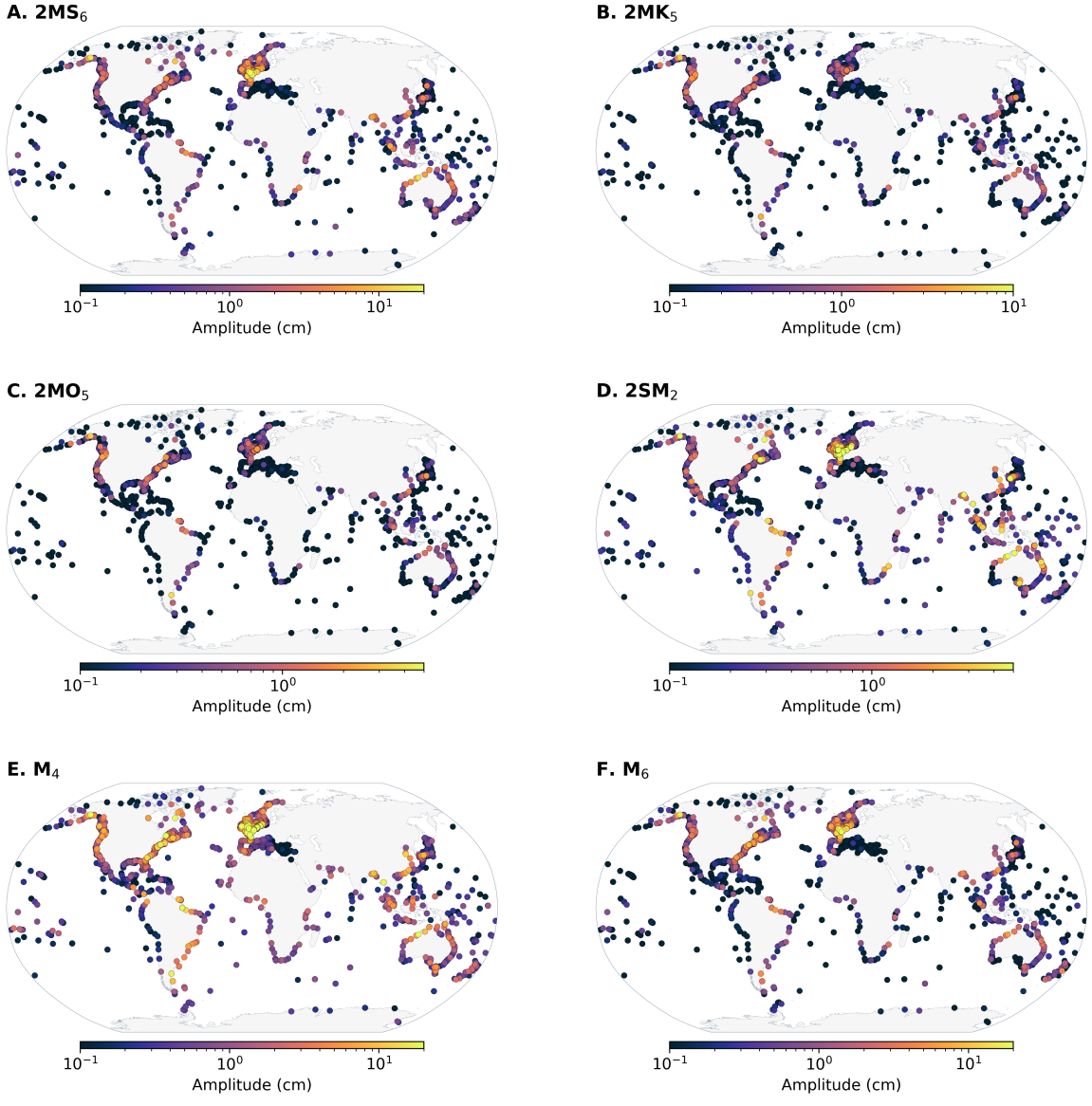

Figure B3. Shallow water tidal constituents taken from TICON-4.

https://doi.org/10.5194/egusphere-2026-346
Preprint. Discussion started: 4 February 2026

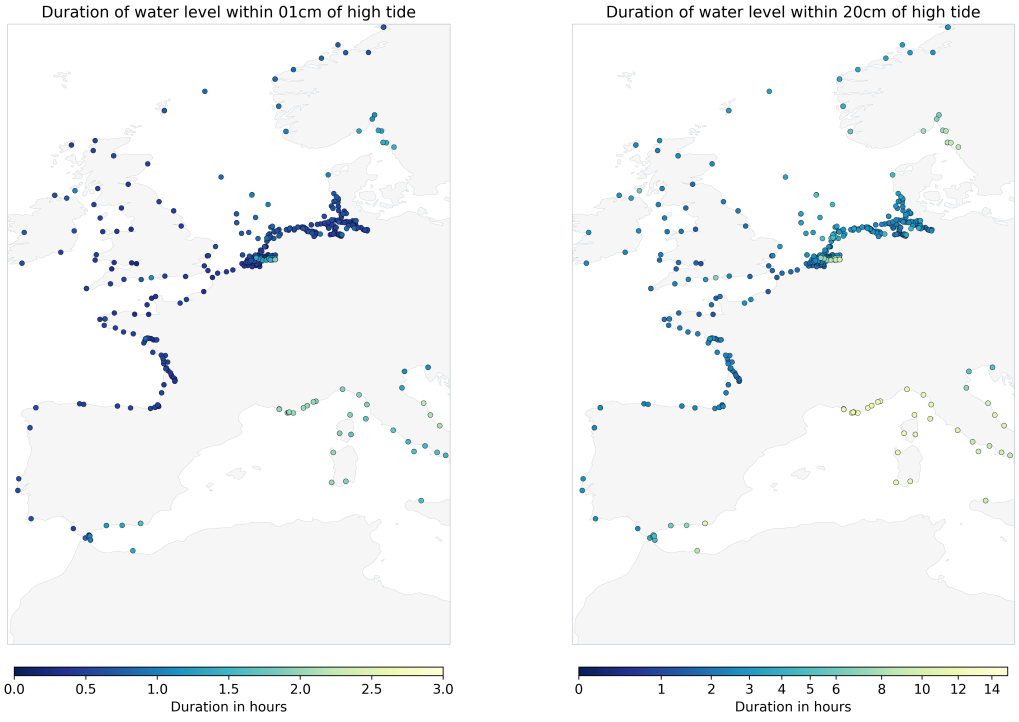

Figure B4. European coastal subset of the flood timing extent.

https://doi.org/10.5194/egusphere-2026-346
Preprint. Discussion started: 4 February 2026

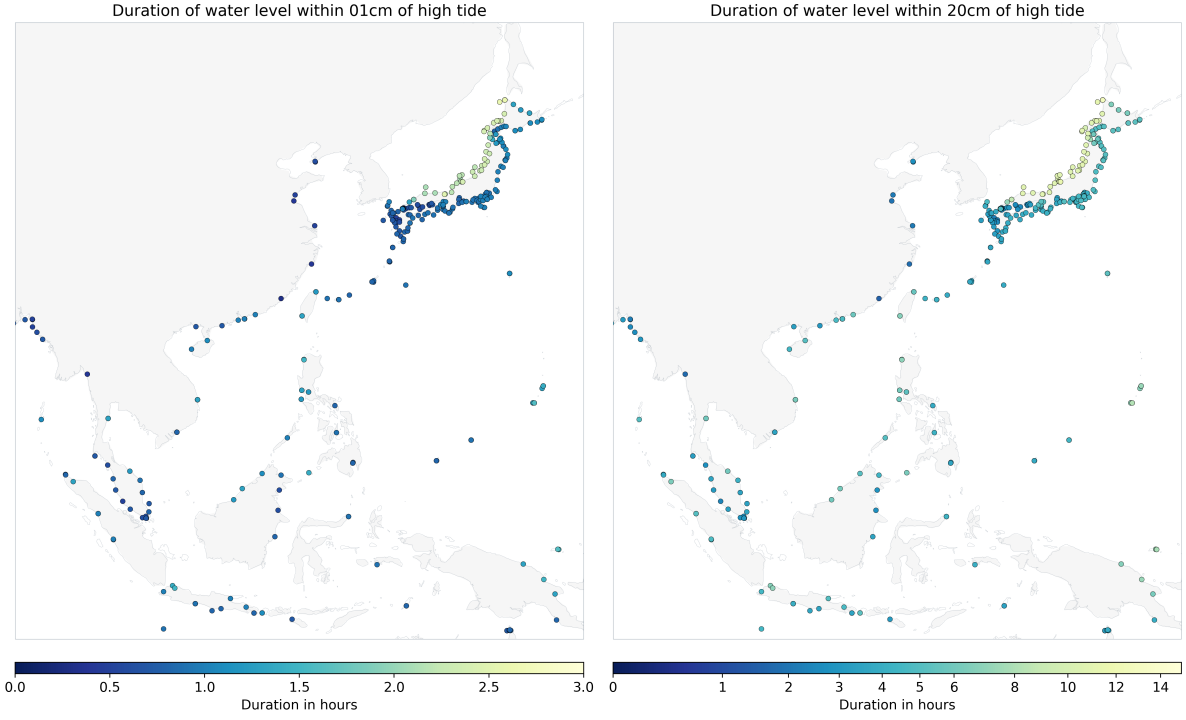

Figure B5. South-east Asian subset of the flood timing extent.

Author contributions. MGHD and RS conceived this study and produced the results of the manuscript. All co-authors provided input on the methods, contributed to the analysis of the results, and the writing of the manuscript.

Competing interests. The contact author has declared that none of the authors has any competing interests.

Acknowledgements. We would like to strongly acknowledge the data centers and individuals who have provided data to GESLA-4, as well as those ensuring the maintenance of these datasets. This work was funded in part by the German Research Foundation (Deutsche Forschungsgemeinschaft DFG) project TIDUS-2 (DE2174/12-2, Project Number 388296632). SAT was funded by the Strategic Environmental Research and Development Program (contract W912HQ24C0020)

https://doi.org/10.5194/egusphere-2026-346
Preprint. Discussion started: 4 February 2026

References

Akan, Ç., Moghimi, S., Özkan-Haller, H. T., Osborne, J., and Kurapov, A.: On the dynamics of the Mouth of the Columbia River: Results from a three-dimensional fully coupled wave-current interaction model, Journal of Geophysical Research: Oceans, 122, 5218–5236, https://doi.org/10.1002/2016JC012307, 2017.

Arbic, B. K.: Atmospheric forcing of the oceanic semidiurnal tide, Geophysical Research Letters, 32, L02 610, https://doi.org/10.1029/2004GL021668, 2005.

Bradshaw, E., Rickards, L., and Aarup, T.: Sea level data archaeology and the Global Sea Level Observing System (GLOSS), GeoResJ, 6, 9–16, https://doi.org/10.1016/j.grj.2015.02.005, 2015.

Burchard, H., Schuttelaars, H. M., and Ralston, D. K.: Sediment trapping in estuaries, Annual Review of Marine Science, 10, 371–395, https://doi.org/10.1146/annurev-marine-010816-060535, 2018.

Buschman, F. A., Hoitink, A. J. F., van der Vegt, M., and Hoekstra, P.: Subtidal water level variation controlled by river flow and tides, Water Resources Research, 45, W10 420, https://doi.org/10.1029/2009WR008167, 2009.

Byun, D.-S., Hart, D. E., Kim, S., and Moon, S.-B.: Classification of monthly tidal envelopes in mixed tide regimes, Scientific Reports, 13, 4786, https://doi.org/10.1038/s41598-023-31657-x, 2023.

Cartwright, D. E.: Tides: A Scientific History, Cambridge University Press, Cambridge, 292pp, 1999.

Codiga, D. L.: Unified tidal analysis and prediction using the U_Tide MATLAB functions, Tech. Rep. URI/GSO Technical Report 2011-01, University of Rhode Island, https://doi.org/10.13140/RG.2.1.3761.2008, 2011.

Coulet, P., Durand, F., Fassoni-Andrade, A., Khan, M. J. U., Testut, L., Toublanc, F., Santos, L. G., Moreira, D. M., and Azevedo, A.: Dynamics of Yearly Maximum Water Levels in the Amazon Estuary, Estuaries and Coasts, 48, https://doi.org/10.1007/s12237-025-01483-7, 2025.

De Ruyter, M.: Captain Inglis and his Tide Machines: The dodging tides of Port Adelaide, from South Australia to the Pacific War at Tarawa, The Mariner's Mirror, 111, 312–325, https://doi.org/10.1080/00253359.2025.2527483, 2025.

Doodson, A. T.: The harmonic development of the tide-generating potential, Proceedings of the Royal Society of London. Series A, 100, 305–329, https://doi.org/10.1098/rspa.1921.0088, 1921.

Doodson, A. T.: Perturbations of harmonic tidal constants, Proceedings of the Royal Society of London. Series A, Containing Papers of a Mathematical and Physical Character, 106, 513–526, https://doi.org/10.1098/rspa.1924.0085, 1924.

Doodson, A. T.: The analysis of high and low waters, International Hydrographic Review, 28, 13–77, 1951.

Doodson, A. T. and Warburg, H. D.: Admiralty Manual of Tides, HMSO, London, 1941.

Dronkers, J. J.: Tidal Computations in Rivers and Coastal Waters, North-Holland, New York, 1964.

Dykstra, S. L., Talke, S. A., Yankovsky, A. E., Torres, R., and Viparelli, E.: Reflection of storm surge and tides in convergent estuaries with dams, the case of Charleston, USA, Journal of Geophysical Research: Oceans, 129, e2023JC020 498, https://doi.org/10.1029/2023JC020498, 2024.

Egbert, G. D. and Ray, R. D.: Tidal Prediction, Journal of Marine Research, 75, https://elischolar.library.yale.edu/journal_of_marine_research/432, 2017.

El-Sabh, M. I. and Murty, T. S.: Technical note: Age of diurnal tide in the World Oceans, Marine Geodesy, 13, 159–166, https://doi.org/10.1080/15210608909379616, 1989.

https://doi.org/10.5194/egusphere-2026-346
Preprint. Discussion started: 4 February 2026

El-Sabh, M. I., Murty, T. S., and Côté, R.: Variations of the age of tides in the global oceans, Marine Geodesy, 11, 153–171, https://doi.org/10.1080/15210608709379557, 1987.

Enríquez, A. R., Wahl, T., Baranes, H. E., Talke, S. A., Orton, P. M., Booth, J. F., and Haigh, I. D.: Predictable changes in extreme sea levels and coastal flood risk due to long-term tidal cycles, Journal of Geophysical Research: Oceans, 127, e2021JC018 157, https://doi.org/10.1029/2021JC018157, 2022.

Familkhalili, R., Talke, S. A., and Jay, D. A.: Tide-storm surge interactions in highly altered estuaries: How channel deepening increases surge vulnerability, Journal of Geophysical Research: Oceans, 125, e2019JC015 286, https://doi.org/10.1029/2019JC015286, 2020.

Feng, X., Tsimplis, M. N., and Woodworth, P. L.: Nodal variations and long-term changes in the main tides on the coasts of China, Journal of Geophysical Research: Oceans, 120, 1215–1232, https://doi.org/10.1002/2014JC010312, 2015.

Foreman, M. G. and Neufeld, E. T.: Harmonic tidal analysis of long time series, The International Hydrographic Review, https://journals.lib.unb.ca/index.php/ihr/article/view/23289, 1991.

Foreman, M. G. G.: Manual for tidal heights analysis and prediction, Tech. Rep. Pacific Marine Science Report 77-10, Institute of Ocean Sciences, 1977.

Foreman, M. G. G. and Henry, R. F.: Tidal Analysis Based on High and Low Water Observations, Tech. Rep. Pacific Marine Science Report 79-15, Institute of Ocean Sciences, 1979.

Gan, M., Pan, H., Chen, Y., and Pan, S.: Application of the Variational Mode Decomposition (VMD) method to river tides, Estuarine, Coastal and Shelf Science, 261, 107 570, https://doi.org/10.1016/j.ecss.2021.107570, 2021.

Garrett, C. J. R. and Munk, W. H.: The age of the tide and the Q of the oceans, Deep Sea Research and Oceanographic Abstracts, 18, 493–503, https://doi.org/10.1016/0011-7471(71)90073-8, 1971.

Geyer, W. R. and MacCready, P.: The estuarine circulation, Annual Review of Fluid Mechanics, 46, 175–197, https://doi.org/10.1146/annurev-fluid-010313-141302, 2014.

Gil, E. and De Toro, C.: New determinations of the ages of tide in the North Atlantic Ocean, Marine Geodesy, 28, 231–249, https://doi.org/10.1080/01490410500204579, 2005.

Godin, G.: The Analysis of Tides, University of Toronto Press, Toronto, 264pp, 1972.

Godin, G.: Frictional effects in river tides, in: Progress in Tidal Hydrodynamics, edited by Parker, B. B., pp. 379–402, John Wiley, New York, 1991.

Green, J. A. M., Green, C. L., Bigg, G. R., Rippeth, T. P., Scourse, J. D., and Uehara, K.: Tidal mixing and the meridional overturning circulation from the Last Glacial Maximum, Geophysical Research Letters, 36, https://doi.org/10.1029/2009GL039309, 2009.

Haigh, I. D., Pickering, M. D., Green, J. M., Arbic, B. K., Arns, A., Dangendorf, S., Hill, D. F., Horsburgh, K., Howard, T., Idier, D., et al.: The tides they are a-Changin': A comprehensive review of past and future nonastronomical changes in tides, their driving mechanisms, and future implications, Reviews of Geophysics, 58, e2018RG000 636, https://doi.org/10.1029/2018RG000636, 2020.

Haigh, I. D., Marcos, M., Talke, S. A., Woodworth, P. L., Hunter, J. R., Hague, B. S., Arns, A., Bradshaw, E., Thompson, P., Domingues, C. M., Piecuch, C. G., Santamaria-Aguilar, D., Navas, F. M., Hermans, T. H. J., Tadesse, M., Rashid, M. M., and Wahl, T.: GESLA Version 3: A major update to the global higher-frequency sea-level dataset, Geoscience Data Journal, 10, 293–314, https://doi.org/10.1002/gdj3.174, 2022.

Haigh, I. D., Marcos, M., Talke, S. A., Hague, B. S., Thompson, P., Nagaraj, M., Beemster, J., Kenwright, C., Martin, A., Wahl, T., Woodworth, P. L., and Hunter, J. R.: GESLA Version 4: Further Enhancements to the Global High-Frequency Sea-Level Dataset, in preparation, 2026.

https://doi.org/10.5194/egusphere-2026-346
Preprint. Discussion started: 4 February 2026

Hart-Davis, M., Dettmering, D., and Seitz, F.: TICON-4: TIdal CONstants based on GESLA-4 sea-level records, https://doi.org/10.17882/109129, 2025.

Hart-Davis, M., Scherer, D., Schwatke, C., Sawyer, A., Pavelsky, T., Ray, R., Dettmering, D., and Seitz, F.: Observing the pulse of tidal rivers: A first global analysis from wide-swath satellite altimetry, https://doi.org/10.21203/rs.3.rs-6825606/v1, 2026.

Hart-Davis, M. G., Dettmering, D., Sulzbach, R., Thomas, M., Schwatke, C., and Seitz, F.: Regional Evaluation of Minor Tidal Constituents for Improved Estimation of Ocean Tides, Remote Sensing, 13, 3310, https://doi.org/10.3390/rs13163310, 2021.

Hart-Davis, M. G., Howard, S. L., Ray, R. D., Andersen, O. B., Padman, L., Nilsen, F., and Dettmering, D.: ArcTiCA: Arctic tidal constituents atlas, Scientific Data, 11, 167, https://doi.org/10.1038/s41597-024-03012-w, 2024.

Hartmann, T. and Wenzel, H.: The harmonic development of the Earth tide generating potential due to the direct effect of the planets, Geophysical Research Letters, 21, 1991–1993, https://doi.org/10.1029/94GL01684, 1994.

Hartmann, T. and Wenzel, H.: The HW95 tidal potential catalogue, Geophysical Research Letters, 22, 3553–3556, https://doi.org/10.1029/95GL03324, 1995.

Hijma, M. P., Engelhart, S. E., Törnqvist, T. E., Horton, B. P., Hu, P., and Hill, D. F.: A protocol for a geological sea-level database, in: Handbook of Sea Level Research, edited by Shennan, I., Long, A. J., and Horton, B. P., Wiley, https://doi.org/10.1002/9781118452547.ch34, 2015.

Hoitink, A. F. and Jay, D. A.: Tidal river dynamics: Implications for deltas, Reviews of Geophysics, 54, 240–272, https://doi.org/10.1002/2015RG000507, 2016.

Horner-Devine, A. R., Jay, D. A., Orton, P. M., and Spahn, E. Y.: A conceptual model of the strongly tidal Columbia River plume, Journal of Marine Systems, 78, 460–475, https://doi.org/10.1016/j.jmarsys.2008.11.025, 2009.

Horsburgh, K. J. and Wilson, C.: Tide-surge interaction and its role in the distribution of surge residuals in the North Sea, Journal of Geophysical Research: Oceans, 112, https://doi.org/10.1029/2006JC004033, 2007.

Hunter, J. R., Woodworth, P. L., Wahl, T., and Nicholls, R. J.: Using global tide gauge data to validate and improve the representation of extreme sea levels in flood impact studies, Global and Planetary Change, 156, 34–45, https://doi.org/10.1016/j.gloplacha.2017.06.007, 2017.

Huthnance, J. M.: On shelf-sea resonance with application to Brazilian M_3 tides, Deep Sea Research Part A. Oceanographic Research Papers, 27, 347–366, https://doi.org/10.1016/0198-0149(80)90031-X, 1980.

Idier, D., Dumas, F., and Muller, H.: Tide-surge interaction in the English Channel, Natural Hazards and Earth System Sciences, 12, 3709–3718, https://doi.org/10.5194/nhess-12-3709-2012, 2012.

Jay, D. A.: Green's law revisited: Tidal long-wave propagation in channels with strong topography, Journal of Geophysical Research: Oceans, 96, 20 585–20 598, https://doi.org/10.1029/91JC01633, 1991.

Jay, D. A.: Evolution of tidal amplitudes in the eastern Pacific Ocean, Geophysical Research Letters, 36, https://doi.org/10.1029/2008GL036185, 2009.

Jay, D. A. and Flinchem, E. P.: Interaction of fluctuating river flow with a barotropic tide: A demonstration of wavelet tidal analysis methods, Journal of Geophysical Research: Oceans, 102, 5705–5720, https://doi.org/10.1029/96JC00496, 1997.

Jay, D. A., Leffler, K., and Degens, S.: Long-term evolution of Columbia River tides, Journal of Waterway, Port, Coastal, and Ocean Engineering, 137, 182–191, https://doi.org/10.1061/(ASCE)WW.1943-5460.0000082, 2011.

https://doi.org/10.5194/egusphere-2026-346
Preprint. Discussion started: 4 February 2026

Jay, D. A., Leffler, K., Diefenderfer, H. L., and Borde, A. B.: Tidal-fluvial and estuarine processes in the lower Columbia River: I. Along-channel water level variations, Pacific Ocean to Bonneville Dam, Estuaries and Coasts, 38, 415–433, https://doi.org/10.1007/s12237-014-9819-0, 2015.

Kästner, K., Hoitink, A. J. F., Torfs, P. J. J. F., Deleersnijder, E., and Ningsih, N. S.: Propagation of tides along a river with a sloping bed, Journal of Fluid Mechanics, 872, 39–73, https://doi.org/10.1017/jfm.2019.331, 2019.

Kukulka, T. and Jay, D. A.: Impacts of Columbia River discharge on salmonid habitat: 1. A nonstationary fluvial tide model, Journal of Geophysical Research: Oceans, 108, https://doi.org/10.1029/2002JC001382, 2003.

Kvas, A., Behzadpour, S., Ellmer, M., Klinger, B., Strasser, S., Zehentner, N., and Mayer-Gürr, T.: ITSG-Grace2018: Overview and Evaluation of a New GRACE-Only Gravity Field Time Series, Journal of Geophysical Research: Solid Earth, 124, 9332–9344, https://doi.org/10.1029/2019JB017415, 2019.

Larson, K. M., Ray, R. D., Nievinski, F. G., and Freymueller, J. T.: The Accidental Tide Gauge: A GPS Reflection Case Study From Kachemak Bay, Alaska, IEEE Geoscience and Remote Sensing Letters, 10, 1200–1204, https://doi.org/10.1109/LGRS.2012.2236075, 2013.

Latapy, A., Ferret, Y., Testut, L., Talke, S., Aarup, T., Pons, F., Woodworth, P. L., and Wöppelmann, G.: Data rescue process in the context of sea level reconstructions: An overview of the methodology, lessons learned, up-to-date best practices and recommendations, Geoscience Data Journal, 10, 396–425, https://doi.org/10.1002/gdj3.179, 2023.

Le Provost, C.: Generation of overtides and compound tides (review), in: Tidal Hydrodynamics, edited by Parker, B. B., pp. 263–295, Wiley, New York, 1991.

Leffler, K. E. and Jay, D. A.: Enhancing tidal harmonic analysis: Robust (hybrid L_1/L_2) solutions, Continental Shelf Research, 29, 78–88, https://doi.org/10.1016/j.csr.2008.04.011, 2009.

Lobo, M., Jay, D. A., Innocenti, S., Talke, S. A., Dykstra, S. L., and Matte, P.: Implementing superresolution of nonstationary tides with wavelets: An introduction to CWT_Multi, Journal of Atmospheric and Oceanic Technology, 41, 969–989, https://doi.org/10.1175/JTECH-D-23-0144.1, 2024.

Lubbock, J. W.: On the tides in the port of London, Philosophical Transactions of the Royal Society of London, 121, 379–415, https://doi.org/10.1098/rstl.1831.0022, 1831.

Lyard, F. H., Allain, D. J., Cancet, M., Carrère, L., and Picot, N.: FES2014 global ocean tide atlas: design and performance, Ocean Science, 17, 615–649, https://doi.org/10.5194/os-17-615-2021, 2021.

Marcos, M., Calafat, F. M., Berihuete, Á., and Dangendorf, S.: Long-term variations in global sea level extremes, Journal of Geophysical Research: Oceans, 120, 8115–8134, https://doi.org/10.1002/2015JC011173, 2015.

Matte, P., Jay, D. A., and Zaron, E. D.: Adaptation of classical tidal harmonic analysis to nonstationary tides, with application to river tides, Journal of Atmospheric and Oceanic Technology, 30, 569–589, https://doi.org/10.1175/JTECH-D-12-00016.1, 2013.

Menéndez, M. and Woodworth, P. L.: Changes in extreme high water levels based on a quasi-global tide-gauge data set, Journal of Geophysical Research: Oceans, 115, https://doi.org/10.1029/2009JC005997, 2010.

Moftakhari, H. R., Jay, D. A., Talke, S. A., Kukulka, T., and Bromirski, P. D.: A novel approach to flow estimation in tidal rivers, Water Resources Research, 49, 4817–4832, https://doi.org/10.1002/wrcr.20363, 2013.

Monahan, T., Tang, T., Roberts, S., and Adcock, T. A. A.: RTide: Automating the Tidal Response Method, Journal of Geophysical Research: Machine Learning and Computation, 2, https://doi.org/10.1029/2024jh000525, 2025.

Munk, W. H.: Abyssal recipes, Deep Sea Research and Oceanographic Abstracts, 13, 707–730, https://doi.org/10.1016/0011-7471(66)90602-4, 1966.

https://doi.org/10.5194/egusphere-2026-346
Preprint. Discussion started: 4 February 2026

Munk, W. H. and Cartwright, D. E.: Tidal spectroscopy and prediction, Philosophical Transactions of the Royal Society of London. Series A, 259, 533–581, https://doi.org/10.1098/rsta.1966.0013, 1966.

Pan, H., Lv, X., Wang, Y., Matte, P., Chen, H., and Jin, G.: Exploration of tidal-fluvial interaction in the Columbia River estuary using S_TIDE, Journal of Geophysical Research: Oceans, 123, 6598–6619, https://doi.org/10.1029/2018JC014146, 2018.

Parker, B. B., ed.: Tidal Hydrodynamics, John Wiley & Sons, New York, ISBN 978-0471514985, papers presented at the International Conference on Tidal Hydrodynamics, November 1988, Gaithersburg, Maryland, 1991.

Parker, B. B.: Tidal Analysis and Prediction, Tech. Rep. Special Publication NOS CO-OPS 3, NOAA, https://doi.org/10.25607/OBP-191, 2007.

Pawlowicz, R., Beardsley, B., and Lentz, S.: Classical tidal harmonic analysis including error estimates in MATLAB using T_TIDE, Computers & Geosciences, 28, 929–937, https://doi.org/10.1016/S0098-3004(02)00013-4, 2002.

Pingree, R. D., Griffiths, D. K., and Maddock, L.: Quarter diurnal shelf resonances and tidal bed stress in the English Channel, Continental Shelf Research, 3, 267–289, https://doi.org/10.1016/0278-4343(84)90012-8, 1984.

Ponte, R. M. and Schindelegger, M.: Seasonal cycle in sea level across the coastal zone, Earth and Space Science, 11, e2024EA003 978, https://doi.org/10.1029/2024EA003978, 2024.

Pouvreau, N.: Trois cents ans de mesures marégraphiques en France: outils, méthodes et tendances des composantes du niveau de la mer au port de Brest, Ph.d. thesis, Université de La Rochelle, La Rochelle, France, 2008.

Pugh, D. and Woodworth, P. L.: Sea-Level Science: Understanding Tides, Surges, Tsunamis and Mean Sea-Level Changes, Cambridge University Press, ISBN 9781107028197, https://doi.org/10.1017/CBO9781139235778, 2014.

Ralston, D. K., Talke, S. A., Geyer, W. R., Al-Zubaidi, H. A., and Sommerfield, C. K.: Bigger tides, less flooding: Effects of dredging on barotropic dynamics in a highly modified estuary, Journal of Geophysical Research: Oceans, 124, 196–211, https://doi.org/10.1029/2018JC014313, 2019.

Ray, R. D.: Secular changes in the solar semidiurnal tide of the western North Atlantic Ocean, Geophysical Research Letters, 36, L19 601, https://doi.org/10.1029/2009GL040217, 2009.

Ray, R. D.: Precise comparisons of bottom-pressure and altimetric ocean tides, Journal of Geophysical Research: Oceans, 118, 4570–4584, https://doi.org/10.1002/jgrc.20336, 2013.

Ray, R. D.: First global observations of third-degree ocean tides, Science Advances, 6, eabd4744, https://doi.org/10.1126/sciadv.abd4744, 2020.

Ray, R. D.: Technical note: On seasonal variability of the M_2 tide, Ocean Science, 18, 1073–1079, https://doi.org/10.5194/os-18-1073-2022, 2022.

Ray, R. D.: Documentation for Goddard Ocean Tide Solution GOT5: Global Tides from Multi-mission Satellite Altimetry, NASA Tech. Memo. 20250002085, Goddard Space Flight Center, Greenbelt MD, https://ntrs.nasa.gov/api/citations/20250002085/downloads/GOT5-TechMemo.pdf, 2025.

Ray, R. D., Loomis, B. D., and Zlotnicki, V.: The mean seasonal cycle in relative sea level from satellite altimetry and gravimetry, Journal of Geodesy, 95, 80, https://doi.org/10.1007/s00190-021-01529-1, 2021.

Robins, P. E., Neill, S. P., Lewis, M. J., and Ward, S. L.: Characterising the spatial and temporal variability of the tidal-stream energy resource over the northwest European shelf seas, Applied Energy, 147, 510–522, https://doi.org/10.1016/j.apenergy.2015.03.045, 2015.

Sammari, C., Koutitonsky, V. G., and Moussa, M.: Sea level variability and tidal resonance in the Gulf of Gabes, Tunisia, Continental Shelf Research, 26, 338–350, https://doi.org/10.1016/j.csr.2005.11.006, 2006.

https://doi.org/10.5194/egusphere-2026-346
Preprint. Discussion started: 4 February 2026

Shalowitz, A. L.: Shore and sea boundaries: Interpretation and use of Coast and Geodetic Survey data, vol. 2, US Department of Commerce, 1964.

Simpson, J. H. and Hunter, J. R.: Fronts in the Irish Sea, Nature, 250, 404–406, https://doi.org/10.1038/250404a0, 1974.

Simpson, J. H. and Sharples, J.: Introduction to the physical and biological oceanography of shelf seas, Cambridge University Press, https://doi.org/10.1017/CBO9781139034098, 2012.

Smith, W. N., Thorpe, S. A., and Graham, A.: Surface effects of bottom-generated turbulence in a shallow tidal sea, Nature, 400, 251–254, https://doi.org/10.1038/22295, 1999.

Stumpf, R. P. and Haines, J. W.: Variations in tidal level in the Gulf of Mexico and implications for tidal wetlands, Estuarine, Coastal and Shelf Science, 46, 165–173, https://doi.org/10.1006/ecss.1997.0276, 1998.

Su, Y. and Jiang, X.: Prediction of tide level based on variable weight combination of LightGBM and CNN-BiGRU model, Scientific Reports, 13, 9, https://doi.org/10.1038/s41598-022-26213-y, 2023.

Sulzbach, R., Wziontek, H., Hart-Davis, M., Dobslaw, H., Scherneck, H.-G., Van Camp, M., Omang, O. C. D., Antokoletz, E. D., Mazurova, E., Thomas, M., and Seitz, F.: Modeling gravimetric signatures of third-degree ocean tides and their detection in superconducting gravimeter records, Journal of Geodesy, 96, https://doi.org/10.1007/s00190-022-01609-w, 2022.

Tabibi, S. M., Geremia-Nievinski, F., Francis, O., and Scherneck, H.-G.: Tidal analysis of GNSS reflectometry applied for coastal sea level sensing in Antarctica and Greenland, Remote Sensing of Environment, 248, 111 959, https://doi.org/10.1016/j.rse.2020.111959, 2020.

Talke, S. A.: How tidal properties influence the future duration of coastal flooding, npj Natural Hazards, 2, 36, https://doi.org/10.1038/s44304-025-00086-3, 2025.

Talke, S. A. and Jay, D. A.: Nineteenth Century North American and Pacific Tides: Lost or Just Forgotten?, Journal of Coastal Research, 29, 118–127, https://doi.org/10.2112/JCOASTRES-D-12-00181.1, 2013.

Talke, S. A. and Jay, D. A.: Changing tides: The role of natural and anthropogenic factors, Annual Review of Marine Science, 12, 121–151, https://doi.org/10.1146/annurev-marine-010419-010727, 2020.

Talke, S. A., de Swart, H. E., and De Jonge, V. N.: An idealized model and systematic process study of oxygen depletion in highly turbid estuaries, Estuaries and Coasts, 32, 602–620, https://doi.org/10.1007/s12237-009-9171-y, 2009.

Talke, S. A., Horner-Devine, A. R., Chickadel, C. C., and Jessup, A. T.: Turbulent kinetic energy and coherent structures in a tidal river, Journal of Geophysical Research: Oceans, 118, 6965–6981, https://doi.org/10.1002/2012JC008103, 2013.

Talke, S. A., Familkhalili, R., and Jay, D. A.: The influence of channel deepening on tides, river discharge effects, and storm surge, Journal of Geophysical Research: Oceans, 126, e2020JC016 328, https://doi.org/10.1029/2020JC016328, 2021.

Thomas, H., Bozec, Y., Elkalay, K., and van Baar, H. J. W.: Enhanced open ocean storage of CO_2 from shelf sea pumping, Science, 304, 1005–1008, https://doi.org/10.1126/science.1095491, 2004.

Thompson, P. R., Widlansky, M. J., Hamlington, B. D., Merrifield, M. A., Marra, J. J., Mitchum, G. T., and Sweet, W.: Rapid increases and extreme months in projections of United States high-tide flooding, Nature Climate Change, 11, 584–590, https://doi.org/10.1038/s41558-021-01077-8, 2021.

Webb, D. J.: On the age of the semi-diurnal tide, Deep-Sea Research and Oceanographic Abstracts, 20, 847–852, https://doi.org/10.1016/0011-7471(73)90006-5, 1973.

Whewell, W.: Essay towards a first approximation to a map of cotidal Lines, Philosophical Transactions of the Royal Society of London, 123, 147–236, https://doi.org/10.1098/rstl.1833.0013, 1833.

https://doi.org/10.5194/egusphere-2026-346
Preprint. Discussion started: 4 February 2026

Woodworth, P. L.: A survey of recent changes in the main components of the ocean tide, Continental Shelf Research, 30, 1680–1691, https://doi.org/10.1016/j.csr.2010.07.002, 2010.

Woodworth, P. L.: The global distribution of the M_1 ocean tide, Ocean Science, 15, 431–442, https://doi.org/10.5194/os-15-431-2019, 2019.

Woodworth, P. L.: Tidal science before and after Newton, in: A Journey Through Tides, edited by Green, M. and Duarte, J., pp. 3–36, Elsevier, https://doi.org/10.1016/B978-0-323-90851-1.00002-9, 2023.

Woodworth, P. L. and Rowe, G. H.: The tidal measurements of James Cook during the voyage of the Endeavour, History of Geo- and Space Sciences, 9, 85–103, https://doi.org/10.5194/hgss-9-85-2018, 2018.

Woodworth, P. L., Hunter, J. R., Marcos, M., Caldwell, P., Menéndez, M., and Haigh, I. D.: Towards a global higher-frequency sea level dataset, Geoscience Data Journal, 3, 50–59, https://doi.org/10.1002/gdj3.42, 2017.

Wunsch, C. and Ferrari, R.: Vertical mixing, energy, and the general circulation of the oceans, Annual Review of Fluid Mechanics, 36, 281–314, https://doi.org/10.1146/annurev.fluid.36.050802.122121, 2004.

Zappa, C. J., McGillis, W. R., Raymond, P. A., Edson, J. B., Hintsa, E. J., Zemmelink, H. J., Dacey, J. W., and Ho, D. T.: Environmental turbulent mixing controls on air-water gas exchange in marine and aquatic systems, Geophysical Research Letters, 34, https://doi.org/10.1029/2006GL028790, 2007.

Zaron, E. D. and Jay, D. A.: An analysis of secular change in tides at open-ocean sites in the Pacific, Journal of Physical Oceanography, 44, 1704–1726, https://doi.org/10.1175/JPO-D-13-0266.1, 2014.